UPPSALA
UNIVERSITET

Digital Comprehensive Summaries of Uppsala Dissertations from the Faculty of Science and Technology 1736

The dynamic emplacement of felsic magma in the upper crust

TOBIAS MATTSSON

ACTA
UNIVERSITATIS
UPSALIENSIS
UPPSALA
2018

ISSN 1651-6214
ISBN 978-91-513-0483-0
urn:nbn:se:uu:diva-363445

Dissertation presented at Uppsala University to be publicly examined in Hambergsalen, Geocentrum, Villavägen 16, Uppsala, Friday, 7 December 2018 at 09:00 for the degree of Doctor of Philosophy. The examination will be conducted in English. Faculty examiner: Prof. Dr. rer. nat. F. Christoph Breitkreuz (Technische Universität Bergakademie Freiberg, Institut für Geologie und Paläontologie, Freiberg, Germany).

Abstract
Mattsson, T. 2018. The dynamic emplacement of felsic magma in the upper crust. *Digital Comprehensive Summaries of Uppsala Dissertations from the Faculty of Science and Technology* 1736. 69 pp. Uppsala: Acta Universitatis Upsaliensis. ISBN 978-91-513-0483-0.

Felsic magma intrudes earth's upper crust through a variety of mechanisms. Magma intrusion growth and shape have mainly been explained in terms of host rock properties and intrusion depth, while considering the magma as an overpressurised fluid. However, volcanologists view a magma as a rheologically evolving fluid, which affects the magma flow in volcanic conduits. This thesis seeks to explore intrusion dynamics during magma emplacement by taking both the magma and the host rock into account. The first part of the thesis investigates the emplacement of the Sandfell laccolith/cryptodome, the Cerro Bayo cryptodome and the Mourne granite pluton. Both cryptodomes grew initially by inflation, which resulted in contact-parallel magma flow. Later during the emplacement, the rim of the intrusions viscously stalled as indicated by brecciation and fracturing in the intrusion rims, which then forced them to grow vertically. Our observations suggest that rheological changes in the magma during intrusion growth may control the shape of the cryptodomes/laccoliths. Previously proposed emplacement mechanisms of the Mourne Mountains granite pluton were tested by investigating host-rock deformation and the surrounding contact-metamorphic aureole. The aureole displays contact-metamorphic segregations that were later deformed by brecciation and shearing. The consistent regional fracture patterns in the pluton roof indicate that it was not widely domed, while the north-eastern wall of the pluton was deflected parallel to the strike of the contact. These observations suggest that multiple mechanisms emplaced the pluton, involving both floor subsidence and deflection of the roof and wall.

The last part of the thesis studies the magma plumbing system to the Holuhraun 2014-15 eruption with mineral and whole-rock geochemistry and thermobarometry. The Holuhraun eruption was accompanied by subsidence in the Bárðarbunga caldera but occurred in the Askja volcanic system. Our results show that the Holuhraun eruption was fed from a vertically extensive magma plumbing system in the Bárðarbunga volcanic system.

The works of this thesis highlight that felsic magma emplacement in the upper crust involves multiple and dynamic mechanisms that control the growth and shape of the intrusion and that the interplay between magma and host-rock properties needs to be considered.

Keywords: laccolith, cryptodome, magma emplacement, magma flow, magma rheology, granite, rhyolite, pluton, AMS, XCT, thermobarometry

Tobias Mattsson, Department of Earth Sciences, Mineralogy, Petrology and Tectonics, Villav. 16, Uppsala University, SE-75236 Uppsala, Sweden.

ISSN 1651-6214
ISBN 978-91-513-0483-0
urn:nbn:se:uu:diva-363445 (http://urn.kb.se/resolve?urn=urn:nbn:se:uu:diva-363445)

"One does not simply walk into Mordor"

Boromir, The Lord of the Rings: The Fellowship of the Ring, New Line Cinema, 2001

List of Papers

This thesis is based on the following papers, which are referred to in the text by their Roman numerals.

I **Mattsson, T.**, Burchardt, S., Almqvist, B.S.G. and Ronchin, E. (2018) Syn-Emplacement Fracturing in the Sandfell Laccolith, Eastern Iceland—Implications for Rhyolite Intrusion Growth and Volcanic Hazards. *Frontiers in Earth Science*, 6: 5.

II **Mattsson, T.**, Burchardt, S., Mair, K. and Place, J. Floor subsidence and roof and wall-rock deformation during the emplacement of the Mourne Mountains granite pluton; Insights from the regional fracture pattern. Manuscript in preparation for *Geosphere.*

III Burchardt, S., Palma, J.O., **Mattsson, T.**, Galland, O., Almqvist, B.S.G., Mair, K., Jerram, D.A. and Hammer, Ø. Multi-stage growth of the Cerro Bayo cryptodome, Chachahuén volcano, Argentina – implications for viscous magma emplacement. Manuscript in preparation for *Journal of Geophysical Research: Solid Earth.*

IV **Mattsson, T.**, Sun, Y., Barker, A.K., Burchardt, S., Hammer, Ø., Palma, J.O., Galland, O., Jerram, D.A., Ofierska, W. and Kuylenstierna, E. Quantifying the crystal cargo of the Cerro Bayo cryptodome, Argentina; A window into pre-emplacement magma processes and storage conditions. Manuscript in preparation for *Bulletin of Volcanology.*

V Geiger, H., **Mattsson, T.**, Deegan, F.M., Troll, V.R., Burchardt, S., Gudmundsson, Ó., Tryggvason, A., Krumbholz, M. and Harris, C. (2016) Magma plumbing for the 2014-2015 Holuhraun eruption, Iceland. *Geochemistry, Geophysics, Geosystems*, 17: 2953–2968.

Personal Contributions

All of the manuscripts in this thesis are the result of the combined efforts of all listed authors. My personal contributions to each paper are described below.

Paper I: 70% of total effort. Steffi Burchardt initiated the study. I formulated the research question together with Steffi Burchardt. I collected samples and field data together with Steffi Burchardt. I analysed the samples with AMS, performed textural analysis and made the 3D model of the Sandfell laccolith for volume calculations. I and Steffi Burchardt interpreted the data and wrote the manuscript with help from the co-authors.

Paper II: 85% of total effort. Steffi Burchardt initiated the study. I formulated the research question. I collected the data with the help of Steffi Burchardt, Karen Mair and a field assistant. I analysed the fracture data, described the contact aureole and made the 3D model of the roof to the Mourne granite pluton. I and Joachim Place performed the scan-line analyses. I wrote the manuscript with the help of all the co-authors.

Paper III: 20% of total effort. Olivier Galland and Steffi Burchardt initiated the study and formulated the research question. I interpreted field magmatic and magnetic fabric data collected by Steffi Burchardt, and the other co-authors. I performed the XCT-scanning together with Øyvind Hammer and analysed the crystal SPO. Steffi Burchardt and I wrote the manuscript with input from all the co-authors.

Paper IV: 35% of total effort. Steffi Burchardt initiated the study. Steffi Burchardt, Abigail Barker and I formulated the research question. I performed the CSD analysis together with help from Weronika Ofierska and Elin Kuylenstierna and interpreted the thermobarometric modelling by Yang Sun and myself. I performed the XCT-scanning together with Øyvind Hammer. I wrote the manuscript together with Yang Sun, Abigail Barker and with help from all the co-authors.

Paper V: 40% of total effort. Steffi Burchardt, Frances Deegan and Valentin Troll initiated the study and formulated the research question. Harri Geiger and I performed microprobe analyses on the samples and interpreted the data. Harri Geiger performed thermobarometric modelling with help from me. I made the petrographic observations and interpreted the geochemical data with help from Harri Geiger. The manuscript was written by Harri Geiger, me, Frances Deegan and Valentin Troll with help from all the co-authors.

Contents

Abbreviations

3D	Three-Dimensional
AMS	Anisotropy of Magnetic Susceptibility
An	Anorthite
BIPIP	British and Irish Palaeogene Igneous Province
CPL	Crossed-Polarised Light
CSD	Crystal Size Distribution
DEM	Digital Elevation Model
EPMA	Electron Probe Microanalyser
FEM	Finite Element Method
ICP-MS	Inductively Coupled Plasma-Mass Spectrometry
ICP-OES	Inductively Coupled Plasma-Optical Emission Spectrometry
Ma	Million years ago
PPL	Plane-Polarised Light
SfM	Structure from Motion
SLB	Strain-Localisation Band
SPO	Shape-Preferred Orientation
SUDL	Southern Uplands-Down-Longford Terrane
UAS	Unmanned Aerial System
XCT	X-ray computed microtomography

1. Introduction

1.1. Scope of the thesis

The sub-volcanic magma production, storage regions and transport channels are referred to as the magma plumbing system (Burchardt, 2018). The location of magma storage, its structure and the processes, such as magma mixing and degassing in the magma plumbing system, shape the eruptive behaviour of a volcano (cf. Cashman and Blundy, 2013; Cassidy *et al.*, 2018).

This thesis is focused on the emplacement and growth of felsic magma chambers in the Earth's upper crust and related processes in the magma plumbing system. The upper crust is anisotropic and displays large temperature contrasts compared to the magma plumbing system, which affects how magma accumulates, forms magma chambers, and is transported (cf. Menand, 2011). Research on magma emplacement in the upper crust has mainly been focused on the processes that make space for magma in the host rock, while the magma is viewed as an over-pressurised fluid (e.g. Morgan, 2018). This largely contrasts the petrologist view of a magma chamber as a shape-less, viscous crystal mush with small melt pockets (Cashman *et al.*, 2017). Moreover, volcanologists view magma as a multiphase fluid with evolving properties during transport prior to eruption (Gonnermann and Manga, 2013; Cassidy *et al.*, 2018). The different views on magma and the magma plumbing system show that there is need for an integrated approach to study the emplacement of magma in the upper crust. To grasp the complex and multi-faceted processes that occur during magma emplacement, this thesis investigates the magma plumbing system both from the perspective of the magma (**Papers I, III, IV, V**), and the magma-host rock interaction (**Papers I, II, III**; Figure 1).

The study of the emplacement of felsic magma chambers helps us understand hazards associated to their emplacement. For example, the emplacement of relatively viscous (often felsic) magma in the shallow magma plumbing system may deform the host volcanic edifice, which can lead to edifice collapse and explosive eruptions (e.g. Lipman *et al.*, 1981; Donnadieu *et al.*, 2001). Furthermore, the investigation of deformation associated with intrusion emplacement could help with the interpretation of deformation associated with active magma intrusions. Research on the shallow

magma plumbing system also has bearing on understanding geothermal heat sources, and the formation of ore deposits (e.g. Richards, 2003; Kennedy *et al.*, 2012, 2018).

The different parts of this thesis are primarily centred on field studies of exposed, 'fossilised' intrusions in the shallow plumbing systems of volcanic and magmatic centres in Iceland (**Paper I**), Northern Ireland (**Paper II and V**), and Argentina (**Paper III and IV**). **Papers I and III** investigate the emplacement of the Sandfell laccolith/cryptodome and the Cerro Bayo cryptodome. Specifically, these studies investigate how magma deformation may be related to rheology changes and affect the growth style of cryptodomes. **Paper II** explores host-rock deformation around the Mourne granite pluton to test different emplacement mechanisms. **Paper IV** studies the processes that occurred before the emplacement of the Cerro Bayo cryptodome with thermobarometric modelling, geochemistry, and petrography.

In **Paper V**, the thesis probes into active volcanism by exploring the products of the Holuhraun 2014 - 15 eruption with thermobarometry and geochemistry. The eruption offered an unprecedented view of the tectono-magmatic processes in the plumbing system of an active Icelandic central volcano (Sigmundsson *et al.*, 2015; Gudmundsson *et al.*, 2016).

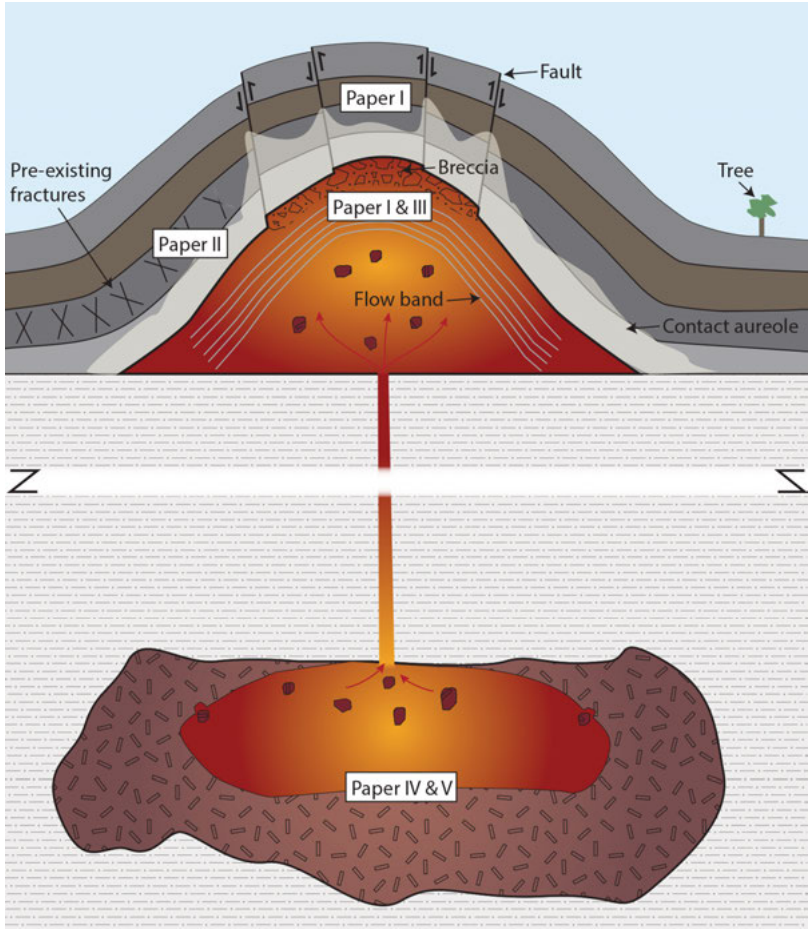

Figure 1. Conceptual sketch of a magma plumbing system. The labels show the parts of the magma plumbing system investigated by the papers of the thesis.

1.2. Emplacement mechanisms of felsic magma bodies in the shallow crust

Here follows an overview of the magma emplacement and intrusion growth mechanisms investigated in **Papers I to III**.

1.2.1. Laccoliths and cryptodomes

Cryptodomes and laccoliths are sub-surface, dome-shaped magma intrusions with a flat floor, that form by pushing away and straining the overlying host rock during the growth of the magma body (Gilbert, 1877; Minakami *et al.*, 1951; Pollard and Johnson, 1973; Lipman *et al.*, 1981; Corry, 1988; Hutton, 1988). Deformation related to laccolith emplacement has generally been

considered to be focused in the host rock, and laccolith growth has therefore primarily been explained in terms of host rock strength and emplacement depth (Pollard and Johnson, 1973; Jackson and Pollard, 1988; Kerr and Pollard, 1998; Bunger and Cruden, 2011; Morgan, 2018).

Laccolith formation is usually confined to the upper ~3-4 km of the crust (Gilbert, 1877; Pollard and Johnson, 1973; Corry, 1988; Roni *et al.*, 2014). Laccoliths that intrude into a volcanic edifice or close to the surface are sometimes called cryptodomes (Minakami *et al.*, 1951). Observed intrusion time-scales of laccolith/cryptodome growth events range from one month to approximately one year (Minakami *et al.*, 1951; Lipman, 1984; Castro *et al.*, 2016). Geochronology and geological mapping of laccoliths show that they can also grow by the intrusion of incremental batches of magma over thousands of years (de Saint-Blanquat *et al.*, 2006; Michel *et al.*, 2008; Breitkreuz *et al.*, 2015).

Laccolith growth has been proposed to occur in three stages: (1) magma intrudes and forms a sill, (2) the sill inflates to a laccolith, (3) the laccolith grows by faulting (or "punching") the host, producing an intrusion sometimes referred to as a "bysmalith" (Gilbert, 1877; Pollard and Johnson, 1973; de Saint-Blanquat *et al.*, 2006). Laccolith growth may terminate and/or skip any of the above-mentioned stages yielding different types of laccolith morphologies. Laccoliths can also form by the stacking of sill intrusions or as several thin intrusions at different depths in crust (Corry, 1988; Rocchi *et al.*, 2010). Exposed cryptodome interiors display extensive concentric deformation within the magma body, such as a brecciated carapace, strong flow-banding and partially brecciated rims (Snyder and Fraser, 1963; Goto and McPhie, 1998; Goto *et al.*, 2000; Stewart and McPhie, 2003).

Deformation in the host associated with laccolith growth involves rotation, uplift, faulting and minor bending and is very localised around the intruding magma body (Corry, 1988; de Saint-Blanquat *et al.*, 2006; Morgan *et al.*, 2008; van Wyk de Vries *et al.*, 2014; Wilson *et al.*, 2016). The different laccolith/cryptodome morphologies result in different host-rock deformation patterns. In case of the inflated-sill type, the host rock should largely drape the domed-shape laccolith (Gilbert, 1877; Hawkes and Hawkes, 1933). In contrast, the host rock to stacked-sill and punched laccoliths is uplifted in a piston-like fashion and should therefore overall retain its original inclination except at the edges of the laccolith where the host rock is rotated and/or faulted (Corry, 1988; Morgan *et al.*, 2008; Wilson *et al.*, 2016).

1.2.2. Cauldron and floor subsidence

Magma emplacement by cauldron subsidence involves subsidence of a block of country rock along a ring-fault within the crust, while magma is transferred along the ring-fault into the space created above the subsiding block (Clough *et al.*, 1909). Cauldron subsidence can be viewed as a subterranean

analogue to caldera collapse (Richey, 1928; Paterson and Fowler, 1993; Cruden and McCaffrey, 2001; Yoshinobu *et al.*, 2003; Burchardt *et al.*, 2012). Originally, the cauldron subsidence emplacement mechanism was considered completely passive, i.e. magma flows into space created by the regional stress field (Richey, 1928; Hutton, 1988; Paterson and Fowler, 1993). The notion that plutons are emplaced either by passive or forceful emplacement is, however, misleading because multiple processes accommodate magma emplacement (e.g. Paterson and Fowler, 1993; Burchardt *et al.*, 2012; Anderson *et al.*, 2017).

Cauldron subsidence is a type of magma emplacement mechanism that involves floor subsidence (Cruden, 1998; Cruden and McCaffrey, 2001). Floor subsidence emplacement is induced by the removal of magma from an underlying reservoir, which triggers the subsidence of the floor of the newly forming magma body along faults (e.g. Cruden, 1998; Cruden and McCaffrey, 2001). These faults may be pre-existing and reactivated weaknesses, such as regional faults (e.g. Holohan *et al.*, 2005). However, in the case of cauldron subsidence, floor subsidence usually occurs along faults that are formed by magmatic activity, such as outward dipping ring-faults with a bell-jar geometry (Anderson, 1937). Another example of an intrusion formed by floor subsidence is a lopolith, where the magma is accommodated by sagging of the floor (Cruden, 1998).

1.3. Internal structures in laccoliths and cryptodomes

A main limitation in studying exposed intrusions to understand their emplacement is the fact that emplacement dynamics need to be deduced from the solidified magmatic rock. The preferred orientation of minerals and other types of fabrics can be used to reconstruct magma flow and the processes that occur during intrusion emplacement (e.g. Benn and Allard, 1989; Paterson *et al.*, 1998; Westerman *et al.*, 2017). However, magmatic fabrics and flow indicators form through different types of processes in the intrusion (see below). One of the main tools used in the thesis to understand magma emplacement is the collection of flow fabric data in the solidified intrusions from e.g. crystal alignment and flow bands, using a variety of techniques. This section summarises magma flow indicators observed in the Sandfell laccolith (**Paper I**) and Cerro Bayo cryptodome (**Paper III**) and interpretations of how they form.

1.3.1. Crystal alignment

Alignment of (shape) anisotropic crystals in a magma has been explained in terms of flow regime. In an expanding flow, crystals are aligned perpendicular to the flow, in a converging flow causes crystals to align parallel to the

flow and in a non-coaxial flow crystals align relative to the velocity gradient of magma flow due to the shear or drag between the magma and e.g. the host rock contact (Figure 2) (Paterson *et al.*, 1998; Geoffroy *et al.*, 2002). This implies that an expanding magma flow forms an oblate fabric (foliation), while a converging flow forms a prolate fabric (lineation). Larger felsic magma bodies often show fabrics parallel to the host rock contacts, which is interpreted as caused by flattening against the roof and wall of the intrusion (e.g. de Saint-Blanquat *et al.*, 2006; Stevenson *et al.*, 2007; Payacán *et al.*, 2014; McCarthy *et al.*, 2015).

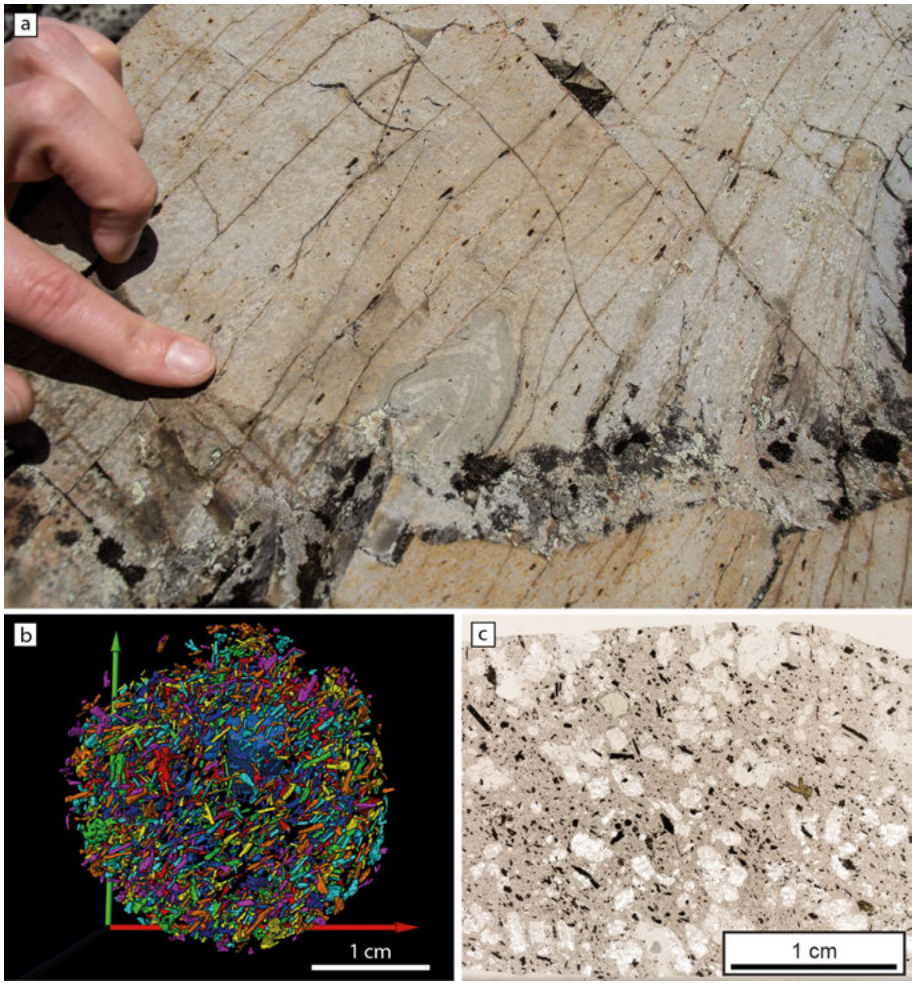

Figure 2. (Previous page). Examples of how mineral alignment was observed/studied in **Papers I and III**. a) The hollows show picked-out aligned plagioclase crystals in the Sandfell laccolith rhyolite. The rhyolite displays a platy parting parallel to the mineral alignment (see fracture perpendicular to rock surface). Also, note the folded flow band in the centre of the photograph. b) Amphibole crystals from a core sample of the Cerro Bayo trachyandesite scanned with XCT. The individual extracted amphibole crystals have been differently coloured to visualize the mineral alignment. The crystals are aligned from the bottom left to top right. c) Thin section of Cerro Bayo trachyandesite (PPL). The dark and green lath-shaped amphibole crystals are aligned from the top left to bottom right in the microphotograph.

1.3.2. Flow bands

Flow bands are planar features in the magma caused by differences in crystallinity and vesicle content (Figures 3 and 4). Flow bands in obsidian lava flows form along shear planes that drive volatile exsolution and crystal growth as an effect of pressure drop and degassing (Tuffen *et al.*, 2003; Castro *et al.*, 2005; Gonnermann and Manga, 2005). In the Sandfell laccolith, the flow bands are related to S-C fabrics, where the flow band represents the C-plane and the groundmass mineral alignment is the S plane (Figure 3d). The flow bands can therefore be considered shear zones in the magma.

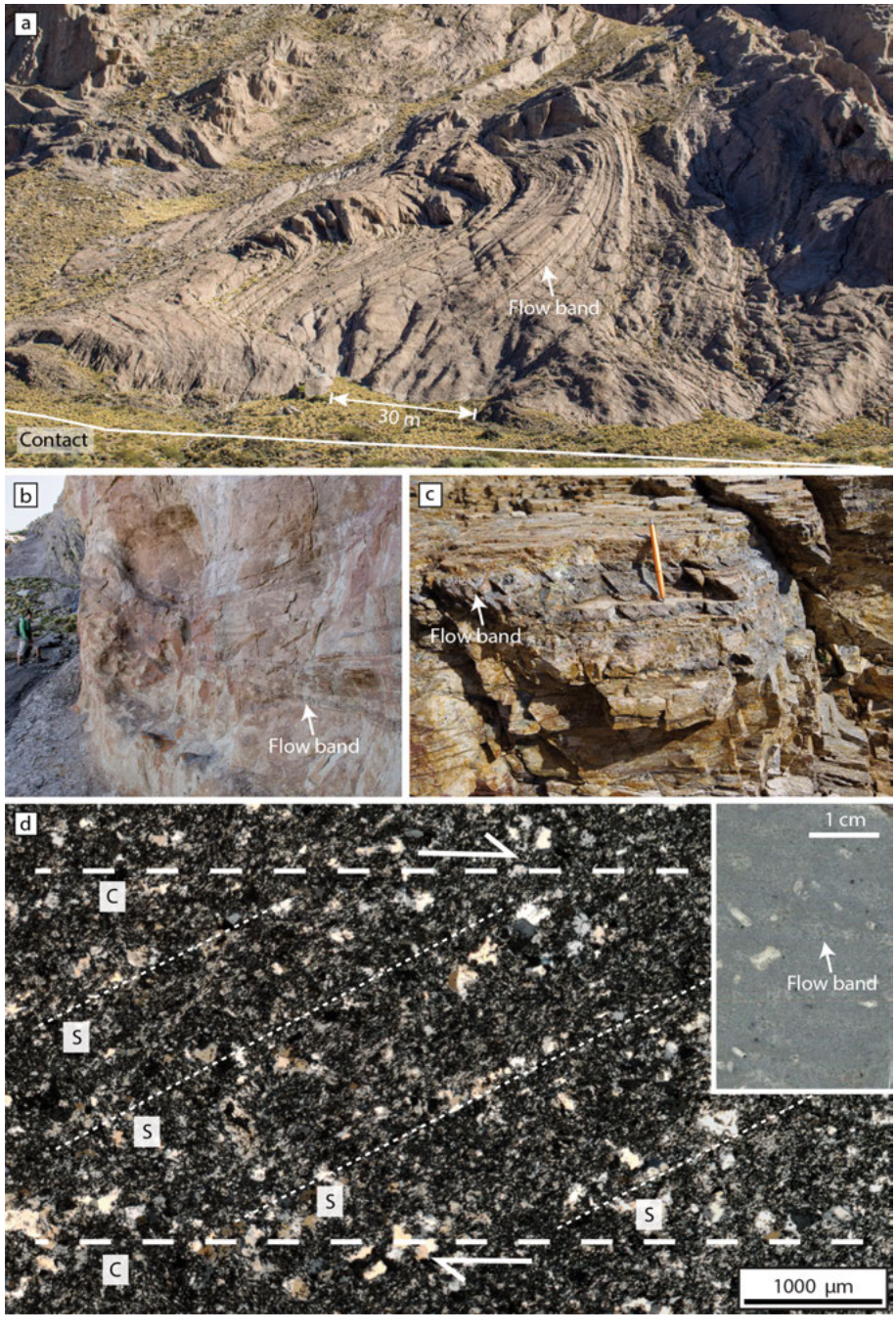
a
Flow band
30 m
Contact
b
Flow band
c
Flow band
d
C
S
S
S
S
C
1 cm
Flow band
1000 µm

Figure 3. (Previous page). Examples of flow banding from the Cerro Bayo cryptodome and the Sandfell laccolith. a) Large-scale flow banding expressed by differential weathering in the southern part of Cerro Bayo. b) Flow bands in the southwestern part of Cerro Bayo. c) Flow bands in the Sandfell rhyolite on the southern slopes of Lower Sandfell. Note the platy parting parallel to the flow bands. d) CPL photomicrographs of S-C fabric in flow-banded rhyolite in the Sandfell laccolith. The sample is from the NW part of the main body of the Sandfell laccolith. Thick dashed white lines designate C planes and thin dashed white lines S planes. The thin section is oriented parallel to the magnetic lineation. The inset displays lighter and darker relatively un-altered flow bands in a cut sample of Sandfell rhyolite.

1.3.3. Strain-localisation bands (shear bands)

During late stages of growth of magmatic intrusions, magma flow in viscous and/or crystal-rich magmas is accommodated along thin shear bands or strain-localization bands (SLBs) in the magma. The SLBs indicate a non-Newtonian magma rheology (Figure 4a) (Smith, 2000; Pistone *et al.*, 2016). For example, in the Sandfell laccolith, SLBs cross-cut the flow bands and have a conjugate geometry (Figure 4a). The SLBs in the Sandfell laccolith are commonly less than 100 μm wide and consist of aligned groundmass microlites. The microlites in the SLBs are not recrystallised, which indicate that the SLBs formed in the magmatic state where the crystal could rotate or, alternatively, originally crystallise within the shear plane. The orientation of SLBs can give an indication of the direction of stress during emplacement of magma (cf. Smith *et al.*, 1993; Závada *et al.*, 2009).

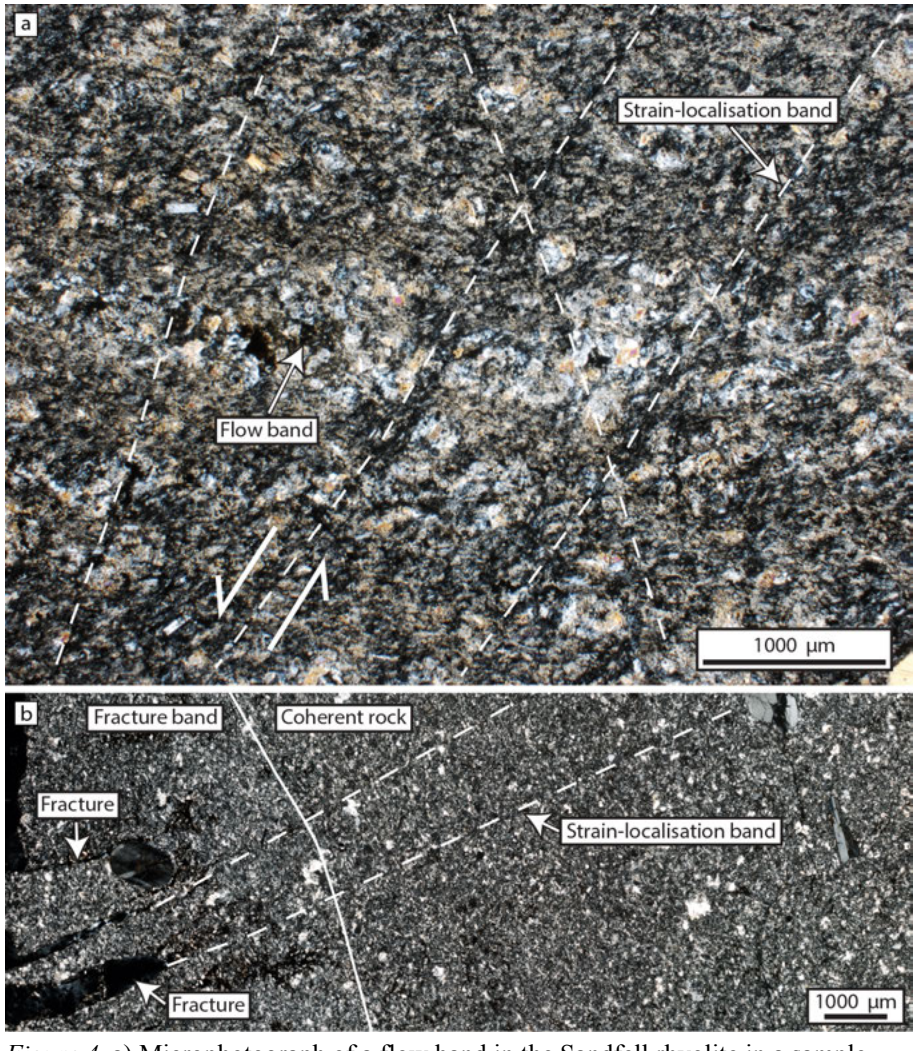

Figure 4. a) Microphotograph of a flow band in the Sandfell rhyolite in a sample collected SE of Upper Sandfell (CPL). The flow bands are characterised by variations in grain-size. Strain-localisation bands (marked by white dashed lines) are oriented oblique to the flow banding. b) Microphotograph of a fracture band and rhyolite groundmass next to fracture bands (CPL). Strain-localization bands (white dashed lines) are observed to transition into fractures. Note the change in groundmass crystallinity and texture closer to the fracture band. The thin sections are either oriented perpendicular to the strike or dip-direction of the flow bands.

1.3.4. Fracture bands

Intensely fractured layers are a common feature in the upper parts of the Sandfell laccolith (Figure 5a-d, **Paper I**), which we term fracture bands due to their banded appearance in the outcrop (Figure 5a, b). Fractured bands have also been observed in Cerro Bayo (Figure 5e, **Paper III**). In the Sand-

fell laccolith, the fracture bands consist of mm- to cm-spaced conjugate fractures, while the fractures are parallel within layers in Cerro Bayo (Figure 5c, e). The fracture bands range from a couple of cm up to metre thicknesses and are commonly separated by coherent, unfractured rock. Microstructures show a close relationship to the strain-localisation bands and the pre-existing flow banding (Figure 4b). This suggests that the heterogeneous layering (in terms of crystallinity and vesicle content) in the magma induced by the flow band formation responded differently to the localised strain by magma compaction (see **Paper I**) and formed during intrusion growth. A parallel arrangement of fractures, such as observed in Cerro Bayo is likely caused by shear between flow banded units during flow. I.e. the magma on either side of the fracture band flowed at different velocities. The conjugate geometry of the fracture bands in the Sandfell laccolith indicates a shear thickening magma rheology (Smith, 2000), and reflects viscous stalling of the magma.

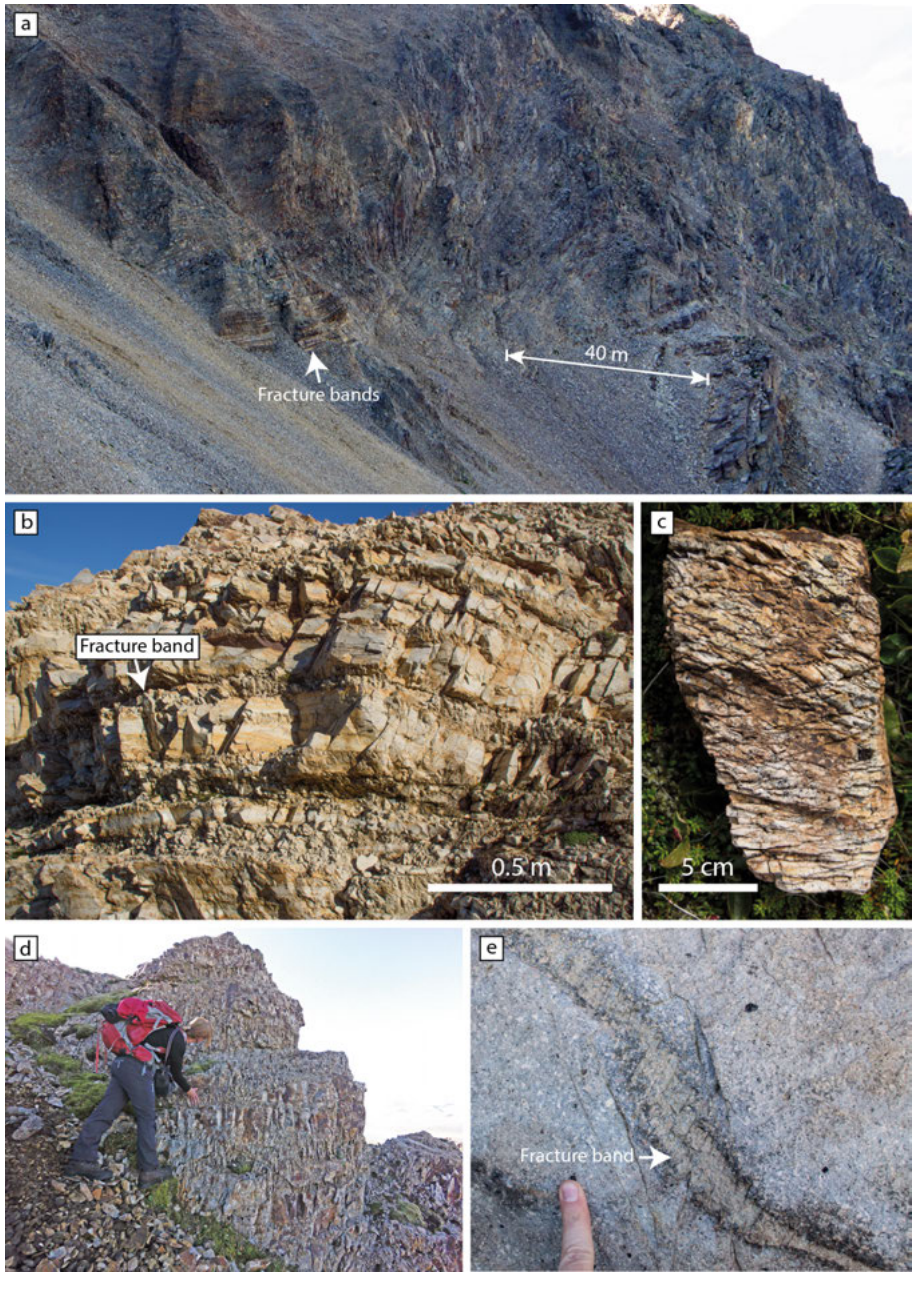
a
Fracture bands
40 m
b
Fracture band
0.5 m
c
5 cm
d
e
Fracture band

Figure 5. (Previous page). a) Fracture banded spur in the northern part of the Sandfell laccolith viewed from the south. The fracture bands give the intrusion a banded appearance due to alteration of the fracture bands. b) Fracture bands separated by coherent rock in an outcrop below Lower Sandfell in the main body of the laccolith. The fracture bands consist of multiple fractures that are oblique to orthogonal to the strike of the bands. Some of the fractures in the bands are rotated. c) Plane-parallel view of a fracture band in a loose rock, showing the typical conjugate arrangement of the fractures. d) Fracture bands below Lower Sandfell. e) Fractured flow band in Cerro Bayo.

1.3.5. Brecciation

Areas close to faulted contacts in the Sandfell laccolith and in the Cerro Bayo cryptodome are brecciated (Figure 6). The breccias consists of cryptodome fragments in a fine-grained rhyolite matrix and are both massive and occur in layers that we interpret as fault gouges (Figure 6a, c, d). In the southern breccia zone of the Sandfell laccolith, there are several faults with slickenlines that dip towards the centre of the intrusion (Figure 6e, f). This observation indicates that the faults are related to the growth of the cryptodome (see **Paper I**). The Cerro Bayo breccia contains lenses of fractured cryptodome rock surrounded by shear zones roughly parallel to the contact between the cryptodome and the host rock (Figure 6b). The breccia zones reflect inflation and faulting of the cryptodome combined with faulting of the host rock.

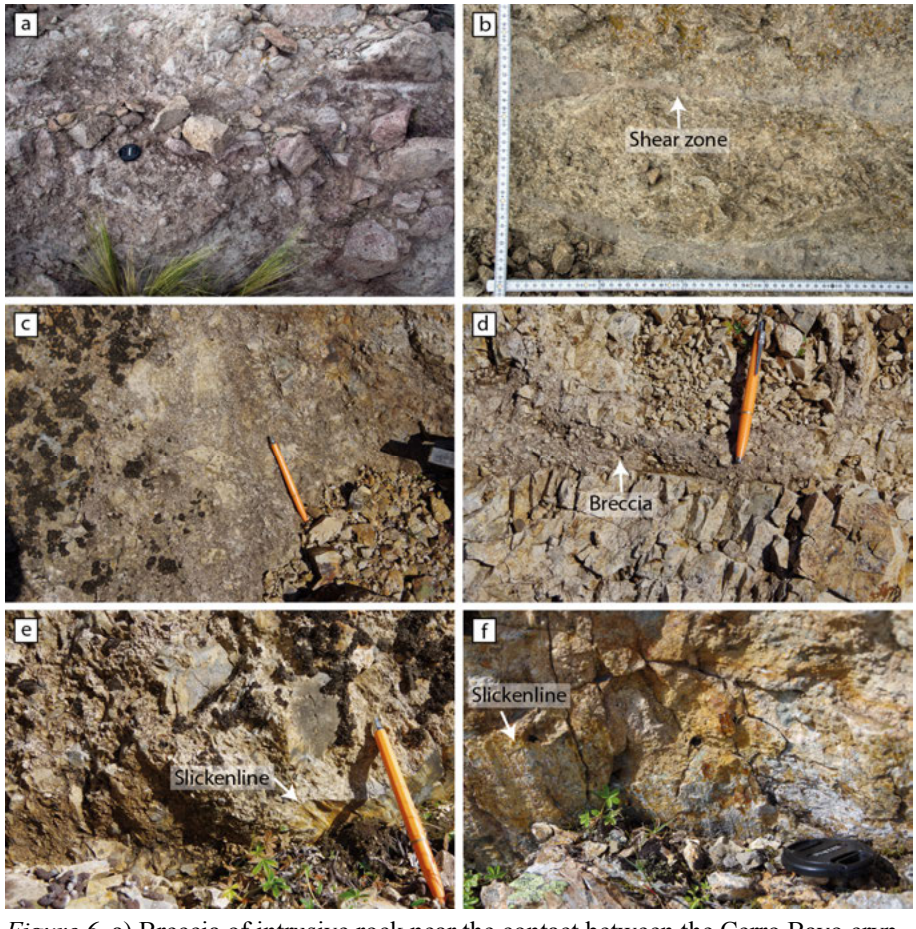

Figure 6. a) Breccia of intrusive rock near the contact between the Cerro Bayo cryptodome and the host rock. Lens cap for scale. b) Shear zone in breccia next to faulted contact of Cerro Bayo. c) Breccia next to the southern faulted contact of the Sandfell laccolith. d) Breccia band in the Sandfell laccolith. We interpret the breccia as fault gouge. e and f) Slickenlines on faults in the breccia zone. The slickenlines dip towards the centre of the main body of the Sandfell laccolith.

2. Geological setting

2.1. Iceland

Iceland is situated at the intersection between the active-rift system of the Mid-Atlantic-Ridge and the Icelandic mantle plume causing an anomalously high magmatic and volcanic activity. The rifting and volcanism in Iceland is primarily focused in the Eastern, Western and Northern Volcanic Zones (Figure 7a) (Sigmundsson, 2006). Each volcanic zone is made up of several volcanic systems that commonly consist of a fissure swarm and a central volcano (Saemundsson, 1979). The Bárðarbunga central volcano in the Bárðarbunga - Veiðivötn volcanic system is situated in the Eastern Volcanic Zone and close to the current centre of the mantle plume (Wolfe *et al.*, 1997). The Bárðarbunga - Veiðivötn volcanic system is one of the most active on Iceland with one eruption every 50 years on average (Larsen and Gudmundsson, 2016).

The concept of a central volcano was developed by G.P.L. Walker and his students after studies on eroded volcanic centres in the East fjords of Iceland and the NW of Scotland (e.g. Walker, 1963, 1966, 1975). A central volcano is assumed to develop due to the formation of a magma chamber close to the surface, which focusses the volcanism in the volcanic system to the area overlying and adjacent to the magma chamber (Walker, 1966). Processes within the shallow magma chamber such as differentiation and partial melting of the surrounding crust generate the characteristic felsic volcanism of a central volcano (Carmichael, 1964; Berg *et al.*, 2018). Central volcanoes also comprise sub-volcanic intrusions, such as cone-sheets and radial dykes that form in the stress field of the shallow magma chambers (Richey *et al.*, 1930; Anderson, 1937; Paquet *et al.*, 2007; Burchardt and Gudmundsson, 2009).

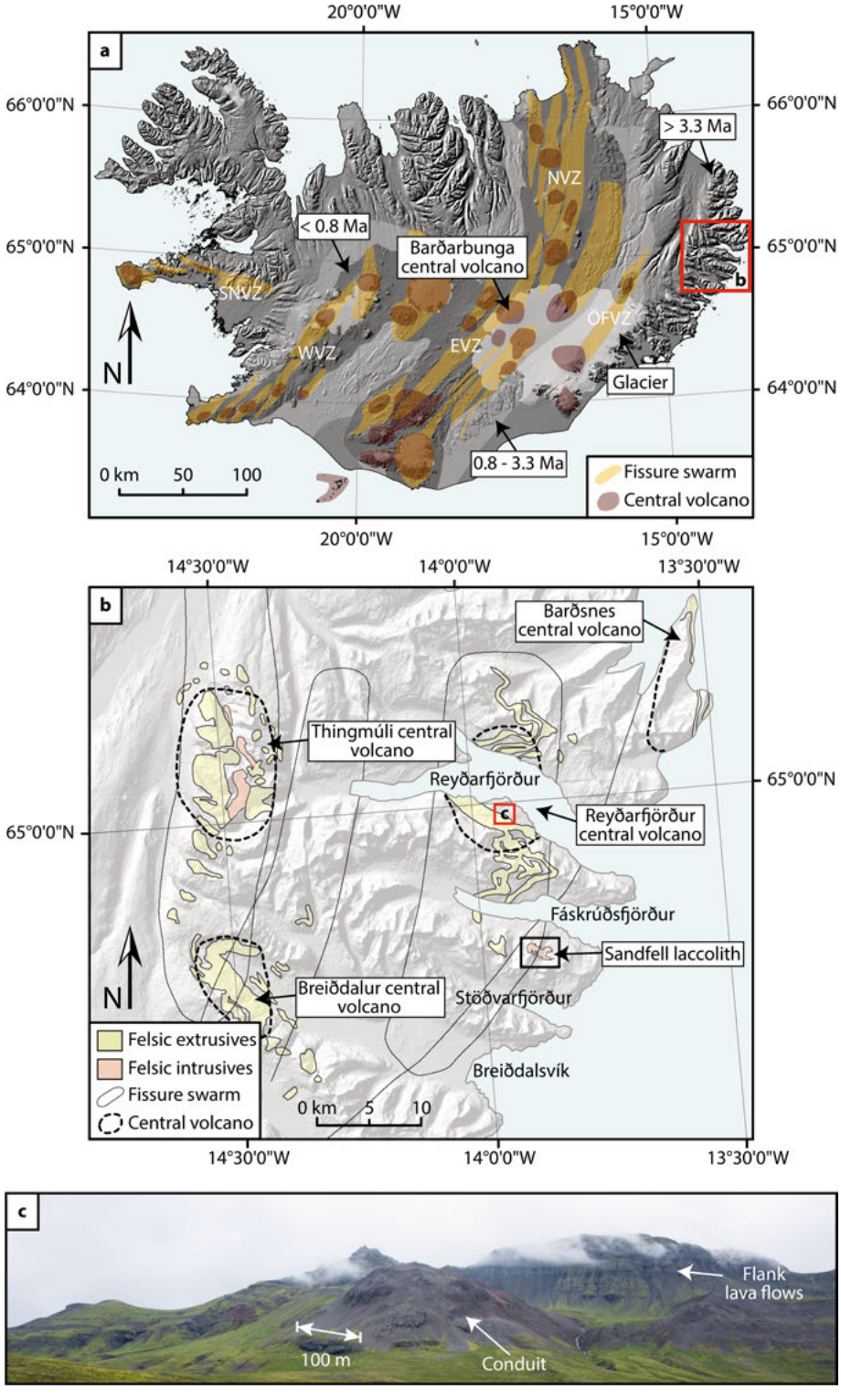
a
20°0'0"W
15°0'0"W
66°0'0"N
65°0'0"N
64°0'0"N
> 3.3 Ma
NVZ
< 0.8 Ma
Barðarbunga central volcano
b
SNVZ
ÖFVZ
WVZ
EVZ
Glacier
N
0 km 50 100
0.8 - 3.3 Ma
Fissure swarm
Central volcano
14°30'0"W
14°0'0"W
13°30'0"W
b
Barðsnes central volcano
Thingmúli central volcano
Reyðarfjörður
c
Reyðarfjörður central volcano
Fáskrúðsfjörður
Sandfell laccolith
Breiðdalur central volcano
Stöðvarfjörður
Felsic extrusives
Felsic intrusives
Fissure swarm
Central volcano
Breiðdalsvík
0 km 5 10
c
Flank lava flows
100 m
Conduit

Figure 7. (Previous page). a) Geodynamic map of Iceland with volcanic systems and central volcanoes (based on data from National Land Survey of Iceland). The Eastern, Western and Northern Volcanic Zones (EVZ, WVZ, and NVZ, respectively) are indicated on the map. The Öræfajökull Flank and the Snæfellnes off-rift Volcanic Zones (ÖFVZ and SNVZ, respectively) are also shown on the map. The different grey-shadings on the map display the age of the rock. Rocks of Upper Pleistocene and Holocene age (<0.8 Ma) are dark grey. Lower Pleistocene and Pliocene rocks (0.8 to 3.3 Ma) are light grey. Neogene rocks older than 3.3 Ma are medium grey. b) Map of exposed fissure swarms and central volcanoes in the East fjords of Iceland. The Sandfell laccolith is located on the flank of the Reyðarfjörður central volcano. The location of the map is shown by the red square in (a). c) Photograph of a conduit in the main eruptive centre of the Reyðarfjörður central volcano. Location of the photograph is shown in (b).

2.1.1. The Reyðarfjörður central volcano

The fjords of Iceland's eastern and south-eastern coast expose a 10 to 12 km thick succession of some of the oldest rocks in Iceland, called the Neogene lava pile (Walker, 1974; Watkins and Walker, 1977; Saemundsson, 1979; Torfason, 1979; Mussett *et al.*, 1980; Einarsson, 1991). The volcanic systems in the eastern fjords became extinct due to dominantly westwards relocations of the rift-axis, eventually ending the volcanic activity in the area (Helgason, 1984; Martin *et al.*, 2011). The extinct central volcanoes and associated fissure swarms are considered direct analogues to the active rift zones on Iceland today (Thordarsson and Höskuldsson, 2002).

The Sandfell laccolith (see **Paper I**) belongs to the Reyðarfjörður central volcano that was active between 12.2 to 11.3 Ma ago (Figure 7b) (Eriksson *et al.*, 2011; Martin *et al.*, 2011). The Reyðarfjörður volcano is located in the area of Fáskrúðsfjörður, Stöðvarfjörður and Reyðarfjörður in eastern Iceland, and has a main eruptive centre in the middle of Reyðarfjörður (Figure 7c) (Gibson, 1963). The eruptive record of the volcano indicates six phases of felsic volcanic activity, each with a different eruptive centre (Gibson, 1963). An eruptive phase commenced with the eruption of an explosive felsic tuff that was followed by effusive felsic, intermediate and basaltic eruptions. The Sandfell laccolith formed in the fourth felsic eruptive phase and intruded and domed the existing lava and silicic pyroclastic flank succession that were emplaced during Phase 2 and 3 of the Reyðarfjörður central volcano, approximately 10 km to the south of the main eruptive centre (Gibson, 1963; Gibson *et al.*, 1966).

2.2. The British and Irish Palaeogene Igneous Province and the Southern Uplands-Down-Longford Terrane

In the Palaeogene, several large volcanoes formed in the (present-day) north-eastern part of the island of Ireland and on the west coast of Scotland (Figure 8). These volcanoes, together with associated lava fields and dyke swarms, constitute the British and Irish Palaeogene Igneous Province (BIPIP) and are associated to the opening of the North Atlantic (Bell and Williamson, 2002; Emeleus and Bell, 2005; Preston, 2009). NW-SE-trending regional dyke swarms in the BIPIP reflect a NE-SW extension during the time period (Jolly and Sanderson, 1995; Macdonald *et al.*, 2009, 2015; Cooper *et al.*, 2012). The study of the well-known igneous centres Ardnamurchan, Mull, Rum, Skye, Slieve Gullion and the Mourne Mountains in the BIPIP introduced and/or popularised some fundamental concepts in volcano research, such as cone sheets, ring-dykes and cauldron subsidence (Bailey *et al.*, 1924; Richey, 1928, 1961; Richey *et al.*, 1930; Le Bas, 1971; Emeleus and Bell, 2005).

The formation of the Mourne Mountains magmatic centre situated on the south-eastern coast of Northern Ireland was one of the final magmatic events of the BIPIP (Richey, 1928; Gibson *et al.*, 1987; Troll *et al.*, 2015). The Mourne magmatic centre is composed of a large granite pluton and a composite dyke swarm, while no extrusive rocks have been linked to the centre (Richey, 1928; Emeleus, 1955; Akiman, 1971; Hood, 1981).

The host rock to the Mourne granite pluton (see **Paper II**) is the Hawick Group greywacke of the NE-SW-trending Southern Uplands-Down-Longford Terrane (Figure 8, SUDL) (Anderson, 2004). The SUDL Terrane formed as an accretionary prism that was folded into steeply-dipping isoclinal folds in front of the advancing Laurentian magmatic arc in the Caledonian orogeny (Anderson and Cameron, 1979; Anderson, 2000). The Hawick group consists primarily of siltstone with quartz and feldspar clasts in a fine-grained groundmass composed of sericite, muscovite, epidote and calcite (Emeleus, 1955).

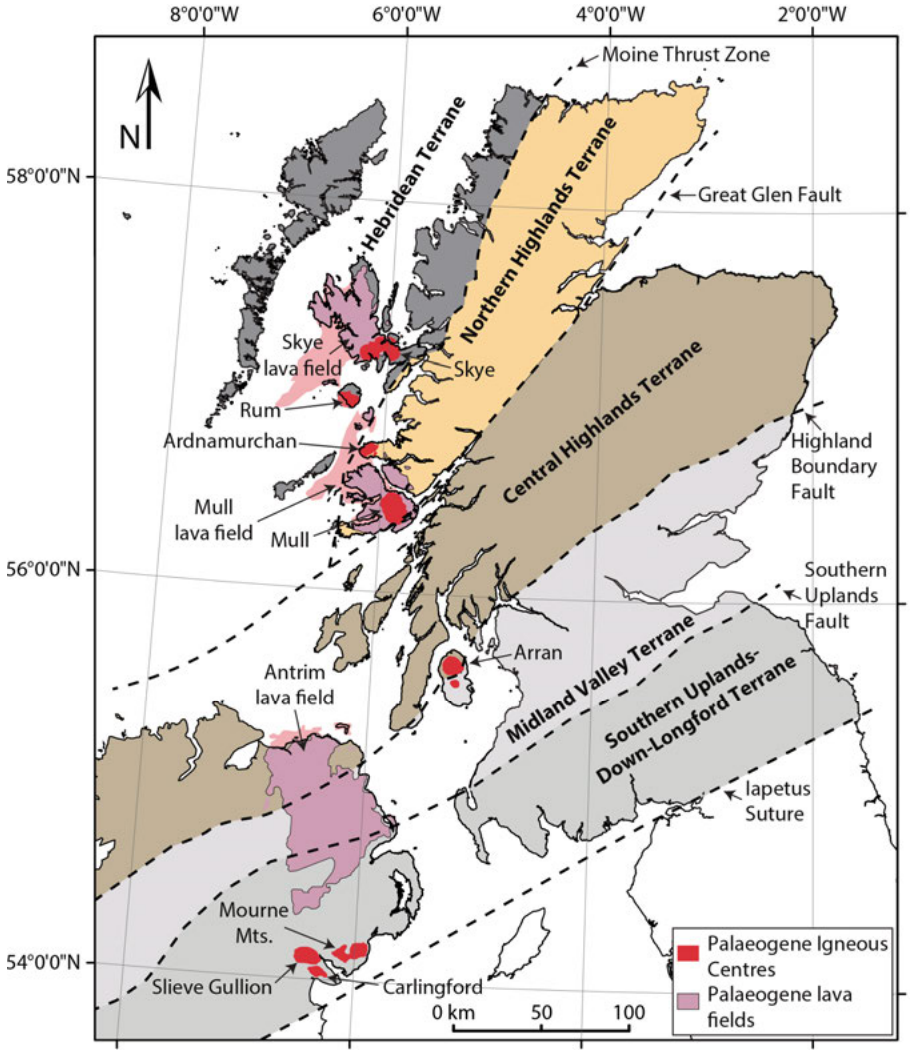

Figure 8. Geological overview map of Scotland and Northern Ireland with tectonic terranes and respective boundaries marked. Palaeogene igneous centres are given in red and associated lava fields in pink. The map is based upon the BGS geology 625k map, with the permission of the British Geological Survey.

2.3. The Chachahuén volcanic centre, Argentina

The Chachahuén volcano is located in the northern part of the Neuquén basin to the east of the Andean volcanic arc (Figure 9). The sedimentary rocks of the Neuquén basin record the early Triassic break-up of Pangaea and early Jurassic to Early Cretaceous thermal subsidence. From the Cretaceous to present, the Neuquén basin has been uplifted in connection to the formation of the Andes (Llambías *et al.*, 2010).

The Chachahuén volcano belongs to the Cenozoic Payenia back-arc volcanic province (Llambías *et al.*, 2010). The Chachahuén volcanic centre comprises multiple phases of volcanic activity that started with the regionally extensive eruption of the Matancilla basalts during early Miocene (Kay *et al.*, 2006; Palma *et al.*, submitted). During the late Miocene, basaltic to rhyolitic effusive to explosive volcanism built up a large volcanic edifice (Vizchachas Formation). The volcanic phase culminated in the formation of a collapse caldera that produced a dacitic ignimbrite at 7.1 ± 0.4 Ma (K/Ar, Pérez and Condat, 1996).

After the caldera collapse, the Chachahuén volcano erupted voluminous block and ash flows, as well as later lava flows (Kay *et al.*, 2006; Palma *et al.*, submitted). The block and ash flows are most likely derived from collapsed volcanic domes and cryptodomes. Several intact cryptodomes and domes are exposed in the Chachahuén centre, the largest of them is the 6.7 ± 0.3 Ma Cerro Bayo (see **Papers III and IV**; Figure 9) (K/Ar, Pérez and Condat, 1996).

An erosional unconformity indicates a hiatus between the post-caldera volcanism and basaltic effusive activity that occurred east of the caldera at 4.85 ± 0.3 Ma (Kay *et al.*, 2006). In the Quaternary, volcanism was restricted to episodic monogenetic basaltic eruptions over a larger area. After the end of magmatic activity, vigorous erosion has removed parts of the flanks and large parts of the interior of the volcano, exposing shallow magmatic intrusions, such as cryptodomes and dykes.

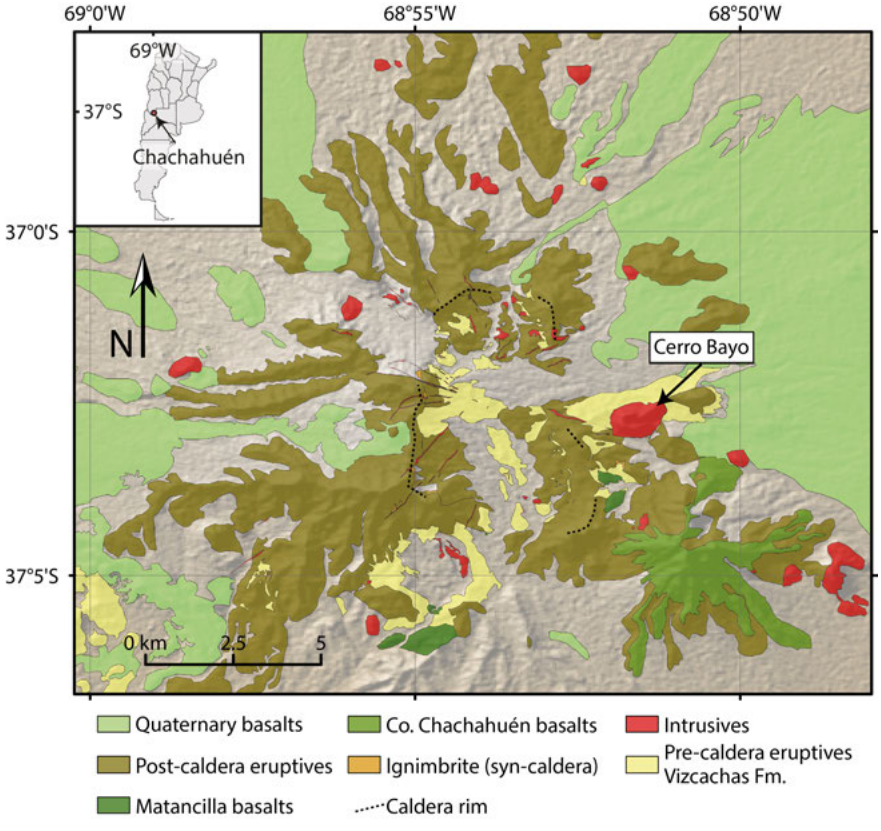

Figure 9. Geological map of the Chachahuén volcano after Palma *et al*. (submitted). Background DEM generated with *GeoMapApp* (http://www.geomapapp.org). The inset shows the location of the Chachahuén volcano in Argentina.

3. Methodology

Here follows a summary of investigative techniques and analytical methods used in the papers of the thesis.

3.1. Structural orientation data collection

Orientation data in **Papers I, II and III** were collected on bedding, fractures, dykes and flow indicators to analyse host-rock deformation and magma flow during magma emplacement with a hand-held analogue compass and/or using the electronic compass in an IPhone 6 with the *Fieldmove Clino* application (www.mve.com/digital-mapping). The electronic measurements were regularly checked in the field with the analogue compass. The electronic compass in an IPhone is accurate to ±10 degrees, but its use speed up the data collection, which allows for better data statistics (cf. Scott *et al.*, 2016; Allmendinger *et al.*, 2017). Lineament data interpreted to represent bedding and fractures were collected in **Paper II** on satellite imagery on beach exposures to complement data measured *in situ*. The orientation data were plotted and contoured with Kamb contouring in *Stereonet 10* (Allmendinger *et al.*, 2012). Data from the host rock to the Mourne granite pluton were also analysed with k-mean cluster analysis in the software *SG2PS* (Sasvári and Baharev, 2014), which limits some of the bias in determining which fractures belong to the same set. We used the Fisher k values generated in *MOVE*™ to determine dispersion within the fracture cluster. Higher Fisher k values indicate a more narrowly clustered set of fractures (Fisher *et al.*, 1993).

3.2. Sample collection and preparation

Oriented samples of the solidified intrusions were collected in the field for magmatic and AMS fabric analyses (**Paper I and III**). Cores 24 mm in diameter × 21 mm long were extracted from the oriented samples at the Swedish Geological Survey, and thin sections were prepared from representative oriented samples for microstructural analyses.

Samples were collected in traverses through the metamorphic aureole to the Mourne granite pluton to investigate small-scale deformation related to granite emplacement (**Paper II**). The traverse samples were cut with a diamond blade to remove weathered parts. Representative samples were selected for thin section preparation. In **Papers IV and V**, the collected samples were crushed/powdered for whole-rock chemical analysis and pieces were cut for thin and thick sections to analyse mineral chemistry. In **Paper V**, plagioclase and olivine glomerocrysts were also picked from the crushed rock and analysed for $\delta^{18}O$.

3.3. Three-dimensional reconstruction of the intrusion shape

Three-dimensional reconstruction was used to estimate the volume of the Sandfell laccolith in **Paper I** and the roof shape of the Mourne granite pluton in **Paper II**. The reconstruction was performed with the software *MOVE 2017.2*™ (www.mve.com) by projecting the mapped contact of the intrusion onto a Digital Elevation Model (DEM) of the topography. Structure contours and/or *in-situ* measurements were then used to extrapolate the dip and dip-direction of the intrusion contact. To calculate the roof surface, several cross-sections were constructed in an evenly spaced grid over the intrusion. In each cross-section, a line representing the intrusion roof was drawn manually taking into consideration the projected dip of contacts and topography. The contact was assumed to lie close to the present-day topography in the intrusion to avoid overestimating its shape and volume (Figure 10). A roof surface of the pluton was subsequently calculated with the Ordinary kriging method using the contacts and the cross-section lines.

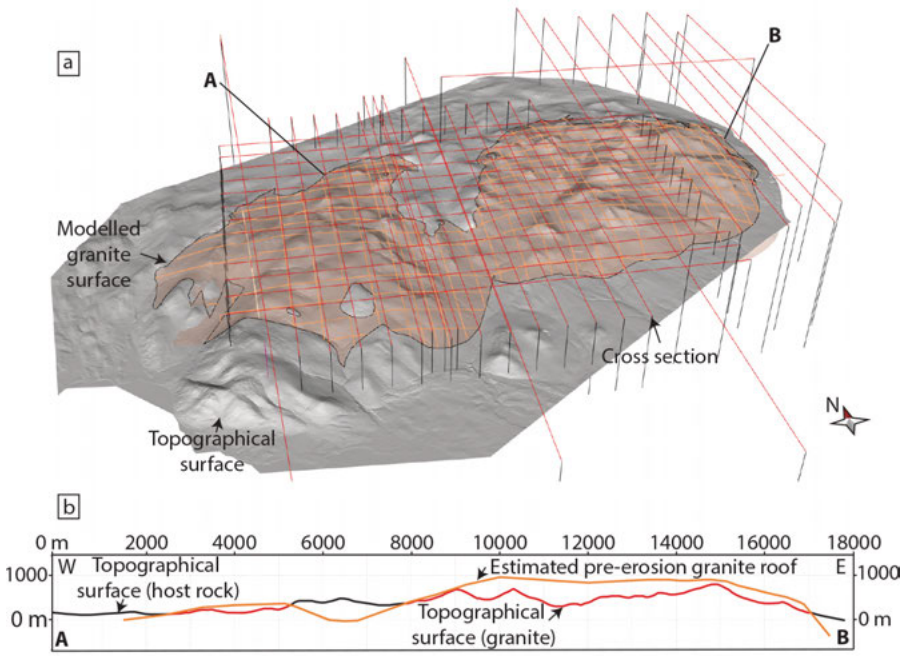

Figure 10. a) Cross-sections used to reconstruct the pre-erosion roof and the topography of the Mourne Mountains (OSNI sheet 253 to 285; *Contains public sector information licensed under the terms of the Open Government Licence v3.0*). See text for details. The orange transparent surface is the reconstructed roof of the Mourne granite pluton. b) Example of a cross-section used to reconstruct the roof. The location and starting and end position of the cross-section is given in (a).

3.4. Photogrammetry and virtual outcrop analysis

A virtual outcrop is a georeferenced photomosaic-textured 3D model of an outcrop, which can be used to remotely study structural features, such as fracture orientations (Figure 11) (cf. Senger *et al.*, 2015). To generate the virtual outcrops, we applied Structure from Motion (SfM) photogrammetry in **Papers II and III**. SfM uses photographs taken on an object from different positions and at different angles to generate a topographical surface (e.g. Bemis *et al.*, 2014). Photographs for photogrammetry were collected using a 24-megapixel DSLR camera with in-built GPS in **Paper II**. One photograph was taken with the camera at chest height and one above the head every metre along the outcrop length. The camera was kept level at a similar distance to the rock face (allowing a fixed focal distance). Overlapping photographs were taken with an Unmanned Aerial System (UAS) also known as a drone in **Paper III**. The images were then processed using the default workflow in the software *Agisoft Photoscan*™ (http://www.agisoft.com/). The quality of photographs was checked with the function 'Estimate Image Quality' and

photographs with a quality <0.5 removed from the image set. Photographs were automatically aligned, and tie points in the photographs were identified with the 'Align Photos' function. The tie points were then used to create a dense point cloud and a mesh surface. The mesh was finally draped with a photomosaic texture created from the photographs generating a 3D 'virtual' outcrop. Ground control points and the photograph position metadata were used to georeference the virtual outcrops.

To analyse the strike and dip of the fractures on the virtual outcrop, the textured surfaces was imported into the software *LIME* v1.0 (http://virtualoutcrop.com/lime) using a local (with accurate scale and orientation) and projected UTM coordinate system. The 'Structural data from 3 points'-tool was used on the outcrop surface to obtain the orientation of measurable fractures (Figure 11).

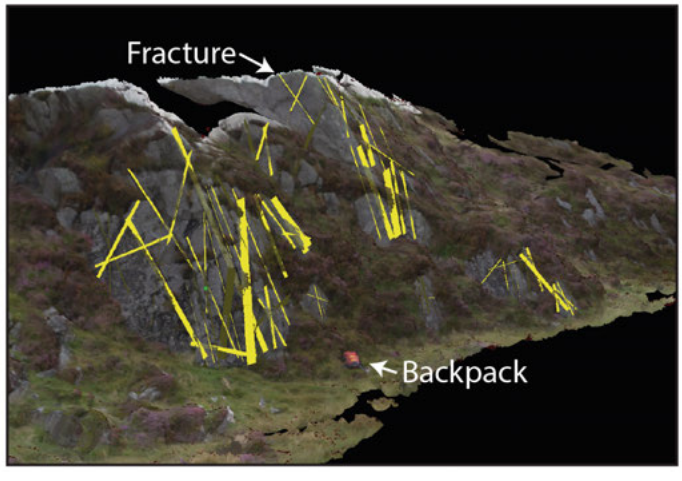

Figure 11. Virtual outcrop (Gruggandoo 1, **Paper II**) of the host rock to the Mourne granite pluton. The yellow planes are mapped fractures.

3.5. Scan line analyses

The fracture intensity in the virtual outcrops of the host rock to the Mourne granite pluton in **Paper II** was studied with the linear scan line method. This implies that one counts all fractures that intersect a chosen line. Fracture orientations in the virtual outcrops were analysed using (virtual) scan lines in *MOVE 2017.2*™ (www.mve.com). The scan lines were drawn manually with a start and endpoint placed horizontally along the long axis of the virtual outcrop. The data were collected along the scan lines by converting the scan lines to wells and counting plane intersections on the well track. Fracture spacing was analysed with a 1 m moving window in *MATLAB*™ (https://www.mathworks.com/products/matlab.html). When measuring frac-

tures along a scan line, a bias is inherently introduced due to the orientation of the scan line. To correct for this bias, we applied a weighting factor (w) (Equation 1):

$$w = \frac{1}{\sin 90 - \beta} \quad (1)$$

Where β is the angle between the pole of the fracture and the azimuth of the scan line (Terzaghi, 1965). Fractures oriented ±15° relative to the scanline were not corrected to avoid large and possibly unrepresentative weighing factors.

3.6. Electron probe microanalyser

To analyse major-element mineral chemistry in **Papers IV and V**, polished thin sections or epoxy pucks of the collected samples were analysed using the Field Emission Gun Electron Probe Microanalyser (FEG-EPMA) JXA-8530F JEOL HYPERPROBE at Uppsala University. The instrument was used in Electron Dispersive Spectroscopy (EDS) mode to identify mineral phases and in Wavelength Dispersive Spectroscopy (WDS) mode for quantitative geochemical analysis on individual mineral grains. For run and analytical conditions, see the respective papers.

3.7. Anisotropy of magnetic susceptibility

Anisotropy of magnetic susceptibility (AMS) analysis was applied on collected samples in **Papers I and III** to study the flow of magma in laccoliths/cryptodomes. The AMS of a sample is analysed in an induced magnetic field and is represented by symmetric second rank magnetic susceptibility tensors. Eigenvalues and eigenvectors are calculated from the susceptibility tensors, which yields three orthogonal, principal axes of susceptibility, $k_1 \geq k_2 \geq k_3$. The magnetic susceptibility principal axes, k_1, k_2, and k_3 can therefore be characterised by an ellipsoid that has a magnitude and orientation (Khan, 1962). The average magnetic susceptibility (K_m) was calculated for every sample using the arithmetic mean of the principal susceptibility axes (Equation 2):

$$K_m = \frac{k_1 + k_2 + k_3}{3} \quad (2)$$

The anisotropy of magnetic susceptibility in a rock can be further described by the parameters P_j, and T, as defined by Jelínek (1981). The corrected degree of anisotropy (P_j,) is given by Equation 3,

$$P_j = \exp\sqrt{2\left((\eta_1 - \eta_m)^2 + (\eta_2 - \eta_m)^2 + (\eta_3 - \eta_m)^2\right)} \quad (3)$$

where $\eta_x = \ln(k_x), x = 1,2,3$ and $\eta_m = \sqrt[3]{\eta_1\eta_2\eta_3}$. The shape factor ($T$) describes the shape of the ellipsoid and is given by Equation 4,

$$T = \frac{2\eta_2 - \eta_1 - \eta_3}{\eta_1 - \eta_3} - 1 \quad (4)$$

T = 1 indicates an oblate fabric, while T = -1 represents a prolate fabric and T = 0 is a triaxial fabric. A P_j value of 1 represents an isotropic fabric, while larger values indicate anisotropy.

The AMS analyses were performed on cores measuring 21 mm × 24 mm in the Laboratory for Experimental Palaeomagnetism at the Department of Earth Sciences, Uppsala University with an Agico Kappabridge MK1-FA. The analysis was carried out in semi-automatic spinning mode in a field of 200 A/m and with a frequency of 976 Hz. The bulk magnetic susceptibility was also measured on magnetic separates from selected samples while heated to 700 °C and cooled back to room temperature in an Argon atmosphere to analyse Curie temperatures of ferromagnetic minerals in the samples. This procedure helps to determine which minerals are responsible for the measured magnetic susceptibility.

The dip and azimuth of a magnetic susceptibility foliation was calculated by fitting a plane to the average k_1 and k_2 axes of a sample. The trend and plunge of the k_1 axis represents the magnetic lineation. Magnetic fabric and anisotropy distribution within the intrusions were analysed with Surfer® from Golden Software (http://www.goldensoftware.com/products/surfer). The magnetic fabric distribution was contoured with Ordinary kriging using UTM location (XY) and the average T (shape factor) or P_j (degree of anisotropy) value as Z for each analysed sample as input for the contouring.

3.8. XCT-scanning

To investigate the mineral fabric (SPO) (**Paper III**) and true 3D CSD (**Paper IV**) in the Cerro Bayo cryptodome magma, samples were analysed with X-ray computed microtomography (XCT or µCT). Five 21 × 24 mm cores were scanned with a Nikon Metrology XT H 225 ST X-ray microtomograph at the Natural History Museum at the University of Oslo (Figure 12). The XCT analyses were run with a 140 kV acceleration voltage, a current of 300 µA, 1 s exposure time, 3016 rotational projections, and a 0.25 mm copper filter. The different minerals in the cores attenuate the X-rays transmitted through the sample, which are collected on a planar 1920×1536-pixel detector. One pixel in the scans was approximately 16 µm long. The processed scans produce a stack of greyscale images, where lighter greyscales correspond to phases of higher densities (Ketcham, 2005a; Jerram and Higgins, 2007). The attenuation of the X-ray beam makes magnetite and amphibole distinguishable in silicate rocks (cf. Figure 2b) (cf. Baker *et al.*, 2012).

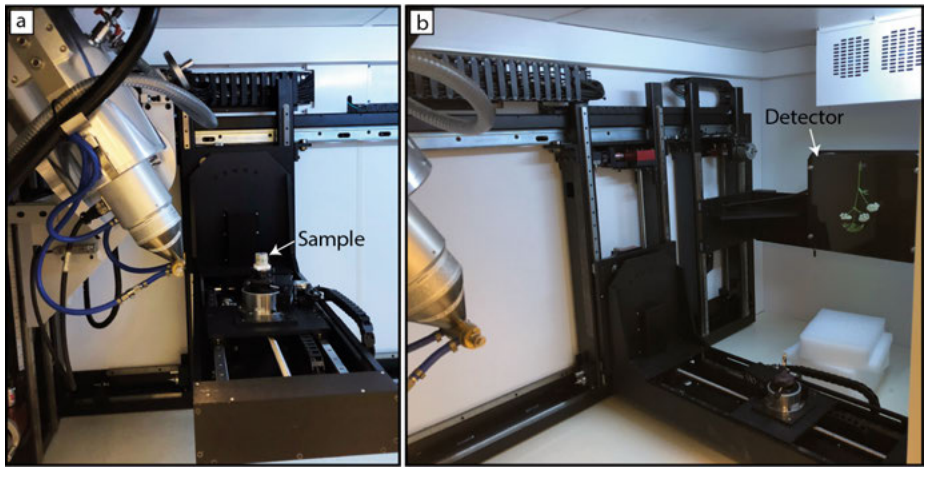

Figure 12. a) Sample mounted in the Nikon Metrology XT H 225 ST X-ray microtomograph. The X-ray gun (to the left) fires X-rays through the rock core that are collected by a detector that is shown in the right-hand side of the photograph in (b).

To analyse crystal SPO in **Paper III**, magnetite and amphibole crystals were separated from the scanned cores using the commercial software Avizo Fire edition (https://www.fei.com/software/amira-avizo/) with greyscale thresholding in the labelling module. During processing of the data in Avizo, spots smaller than between 1000 and 4000 voxels (volume pixels) were removed to limit noise from breakdown rims on crystals. The orientations of the long axis of the separated volumes (likely representing crystals) were imported as lineation data into *Stereonet 10* (Allmendinger *et al.*, 2012). The shape preferred orientation (SPO) of the amphibole and magnetite crystals in a sample were analysed with Fisher statistics in *Stereonet 10* to calculate eigenvalues and eigenvectors of the long-axes SPO of the crystal populations.

The software *Blob3D* (Ketcham, 2005b) was used to analyse the crystal shapes (**Paper III**) and CSD (**Paper IV**) of magnetite and amphibole. Only 300 slices or ~20 % of the scanned volume of the cores were processed, and crystals smaller than 2500 voxels for amphibole and 1000 voxels for magnetite were not analysed to speed up processing and to limit noise due to crystal breakdown rims.

3.9. Crystal Size Distribution

Crystal Size Distribution (CSD) is commonly used to quantitatively determine the number of crystals of a specific size range per unit volume and is traditionally displayed on a plot of population density (n, mm^{-4}) vs. apparent crystal size (L, mm) (Cashman and Marsh, 1988; Marsh, 1988). The slope of

the CSD of a crystal population ($-1/G\tau$, mm^{-1}) gives the characteristic crystal lengths ($G\tau$), as well as the nuclei population density (n^0, mm^{-4}) from the y-intercept. The CSD slope can provide information about nucleation and crystal growth rate (G, mm day^{-1}) assuming a residence time (τ, days). Patterns within CSDs are also important as these can be used to infer magmatic processes such a crystal mixing, textural coarsening and fragmentation (Cashman and Marsh, 1988; Marsh, 1988, 1998; Cashman, 1990; Higgins, 1998; Turner *et al.*, 2003; Higgins and Roberge, 2003; Jerram *et al.*, 2003, 2009; Mock *et al.*, 2003; Muir *et al.*, 2012; Riker *et al.*, 2015). Measurements of the CSD are made using both 2D (thin/polished section) and 3D (e.g. serial sections, XCT) (see e.g. Jerram and Higgins, 2007; Jerram *et al.*, 2018). A sample size of ~250 crystals is required to get a true reflection of the CSD population and the shape of the crystals (Mock and Jerram, 2005; Morgan and Jerram, 2006).

To analyse CSDs in Cerro Bayo, plagioclase and amphibole phenocrysts were traced manually on plane and crossed-polarised thin sections. The shape of traced crystal intersection (long and short-axis) and area were extracted from binary images with the image processing software *ImageJ* (e.g. Schneider *et al.*, 2012). The data was corrected for intersection bias and plotted with *CSDcorrections 1.6* (Higgins, 2000). Crystal axis ratios for shape correction were estimated with *CSDSlice* (Morgan and Jerram, 2006). The CSDs of extracted amphibole crystals from the XCT-scans of Cerro Bayo cores were also analysed to complement the CSDs from data collected on thin sections.

3.10. Thermobarometric and thermodynamic modelling

Thermobarometry can be used to estimate the crystallisation pressure and temperature of minerals in a magma. Different thermobarometers were employed to the magmatic systems in **Papers IV and V**. In **Paper IV**, we employed single amphibole thermobarometers (Ridolfi *et al.*, 2010; Ridolfi and Renzulli, 2012), a amphibole-melt thermobarometer (Putirka, 2016) and a clinopyroxene-melt thermobarometer (Putirka, 2008). In **Paper V**, we used OPAM melt thermobarometry (Yang *et al.*, 1996; Kelley and Barton, 2008), a clinopyroxene single-crystal thermobarometer (Putirka, 2008), a pyroxene-melt thermobarometer (Putirka, 2008), and a plagioclase-melt thermobarometer (Putirka, 2005, 2008). The mineral-melt thermobarometers are calculated based on the exchange of components between the mineral and melt in equilibrium. Equilibrium tests between crystal and melt are used to find suitable melts as input (Putirka, 2008). The mineral-melt thermobarometric formulations also require input of water content. In **Paper IV**, we used the plagioclase hygrometer of Waters and Lange (2015) to estimate the water content of the crystallising magma, while literature values for water content in

Icelandic magma were used as input in the mineral-melt thermobarometers in **Paper V**. To convert pressure to depth we used Equation (5):

$$\frac{P}{\rho \times g} = Depth(m) \quad (5)$$

Where P is the pressure (Pascal), ρ (kg m^{-3}) the bedrock density and *g* is the acceleration due to gravity (9.81 m s^{-2}). Average crustal densities in the study areas were used for the conversion.

3.11. Additional methods used in the manuscripts

The papers in this thesis also employ additional methods and data acquired from co-workers and commercial labs. These methods include Finite-Element Method (FEM) modelling (**Paper I**), ICP-MS and ICP-OES (**Paper IV and V**) and stable isotope analyses (**Paper V**) and are described in the respective manuscripts.

4. Summary of papers

4.1. Paper I

Syn-Emplacement Fracturing in the Sandfell Laccolith, Eastern Iceland—Implications for Rhyolite Intrusion Growth and Volcanic Hazards

The Sandfell laccolith in Fáskrúðsfjörður, eastern Iceland intruded at a depth of about 540 m below the palaeosurface on the flank of the Reyðarfjörður central volcano (see Section 2.1.1; Hawkes and Hawkes, 1933; Gibson *et al.*, 1966). The shallow emplacement depth implies that the Sandfell laccolith can also be considered a cryptodome. To investigate the growth of the Sandfell laccolith, we employed AMS, magma flow indicator mapping, microstructural analysis, 3D intrusion reconstruction and FEM modelling.

The formation of the Sandfell laccolith distinctly domed the host rock, which consists of basaltic lava flows and felsic tuffs and ignimbrites (Hawkes and Hawkes, 1933; Gibson, 1963; Gibson *et al.*, 1966). No internal contacts were observed within the intrusion, indicating that the Sandfell laccolith formed in a single intrusive event. Concentric flow bands and associated S-C fabrics in the Sandfell laccolith reveal contact-parallel magma flow during the initial stages of cryptodome inflation. The magma flow fabrics in the upper part of the main body are overprinted by SLBs, and more than one third of the volume of the Sandfell laccolith displays concentric, intensely fractured layers. A dominantly oblate magnetic fabric in the fractured areas, conjugate geometry of the SLBs, and the fractures in the fracture layers demonstrate that the SLBs and the fracture layers formed by intrusive stresses (Figure 13). Moreover, the fracture bands show that the rhyolite magma underwent a rheological transition from a flowing magma to a stalled viscous crystal mush. We propose that rim solidification was a result of rapid crystallisation caused by a pressure drop due to strain localization and fracturing in the magma. The outer solidified rim of the Sandfell laccolith was subsequently deformed and uplifted in a similar fashion to the host rock. The solidification of the rim of the intrusion forced later intruding magma to flow vertically by faulting and uplifting (punching) the solidified rim of the intrusion.

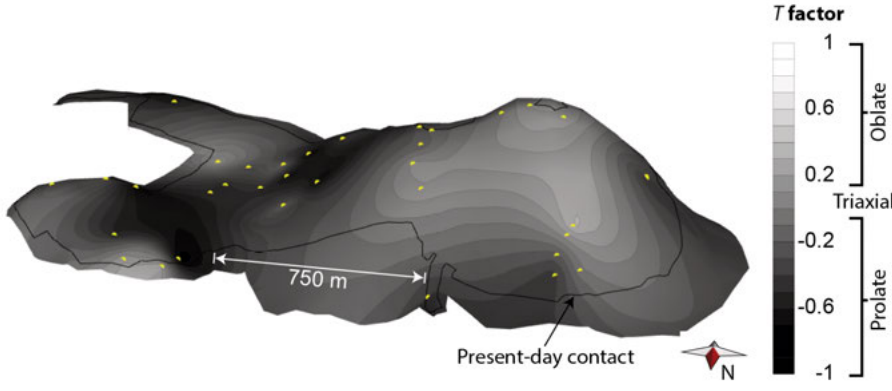

Figure 13. Contoured map of *T* factor of the measured anisotropy of magnetic susceptibility fabric draped on the reconstructed roof surface of the Sandfell laccolith. In the western part of the main body of the Sandfell laccolith, the magnetic fabric is dominantly oblate, while dominantly prolate in the eastern part. The contour map displays a correlation between magnetic fabric shape and elevation in the main body of the Sandfell laccolith indicating that earlier emplaced magma was compacted by later emplaced magma. The yellow points are the sample locations used for contouring with the Ordinary kriging method and the black line indicates the present-day contact between the Sandfell laccolith and its host rock.

4.2. Paper II

Floor subsidence and roof and wall-rock deformation during the emplacement of the Mourne Mountains granite pluton; Insights from the regional fracture pattern

The Mourne Mountains consists of five successive granite intrusions emplaced into Silurian Hawick Group sediments of the Caledonian Southern Uplands-Down-Longford Terrane (SUDL) (see Section 2.2; Anderson, 2000, 2004; Cooper and Johnston, 2004). The host rock to the Mourne Mountains granite pluton experienced multi-phase deformation during the Caledonian orogeny (Anderson, 1987, 2000) and is generally not well exposed in the Mourne Mountains. Consequently, there has been some debate about the mechanism of granite emplacement.

Richey (1928) suggested that the Mourne granites were emplaced by cauldron subsidence, because the host rock close to the Mourne granite pluton did not display distinct deformation related to granite emplacement, and the exposed intrusion contacts are mainly discordant to the host-rock bedding (i.e. the granites truncate the bedding). Cauldron subsidence encompasses subsidence of a block of country rock along a ring-fault within the crust, while magma is transferred along the ring-fault into the space created above the subsiding block (see Section 1.2.2; Clough *et al.*, 1909). Two re-

cent AMS (anisotropy of magnetic susceptibility) studies on the Mourne granites by Stevenson *et al.* (2007) and Stevenson and Bennet (2011) interpreted the intrusions as successively emplaced laccoliths (or bysmaliths). They supported their interpretation based on a flat-lying magnetic mineral fabric in the centre of the intrusion, shallowly plunging fabric at the contacts, the divergent strikes of the SUDL strata along the granites' north-eastern boundary (Hood, 1981), and remapping of the granites (Meighan *et al.*, 1984). Laccolith intrusions form by inflation and dome their host rocks (see Section 1.2.1; Gilbert, 1877; Pollard and Johnson, 1973; Corry, 1988).

In this study, we investigate the emplacement mechanism of the Mourne granite pluton using the regional fracture pattern in the host rock as proxies for deformation. We also describe microstructures in the aureole to constrain timing of deformation related to the alteration induced by granite emplacement. Our approach includes fracture-data rotation analysis based on the dip and strike of the contact to shed more light on granite emplacement from the associated host-rock deformation perspective. The fracture data was dominantly collected on roof exposures on the edge of the pluton. If the Mourne granite pluton was emplaced as successive laccoliths, the regional fracture sets should be rotated to reflect laccolith inflation. If cauldron subsidence emplaced the granites, the fracture sets should be similar in all host-rock localities surrounding the pluton.

The dip and azimuth of the regional fractures are very consistent on the roof of the intrusion and can be separated into four steeply-dipping sets dominantly striking SE, S, NE, and E, which rules out pluton-wide doming. In contrast, fracture orientations in the wall to the granites in the NE show rotation due to contact-strike parallel shear.

Contact-metamorphic segregations in the aureole to the Mourne granite pluton are displaced by small faults. Interestingly, this observation indicates that the initial emplacement of magma did not cause significant deformation, while later granite emplacement is associated with deformation. The aureole therefore records multiple emplacement mechanisms for the granites. The displaced and brecciated contact-metamorphic segregations (Figure 14) and the occurrence of cataclasite and breccia in the Glen River and Bloody Bridge River traverses indicate that granite emplacement was associated with significant shear on the north-eastern wall of the pluton (Figure 14a, b). Our observations in the aureole strongly suggest that neither cauldron subsidence emplacement, which would not cause deformation of the roof and wall, nor laccolith emplacement, which would be associated with deformation throughout pluton emplacement can solely explain the deformation pattern in the aureole.

Based on the north-eastward inclined granite-granite contacts, sub-vertical joints in the granites inclined to the west, and the westward younging succession of the granites, we propose that multiple mechanisms involving asymmetric 'trap-door' floor subsidence and deflection of the north-eastern

wall of the intrusion parallel to a propagating ring-dyke accommodated the emplacement of the granites (Figure 15).

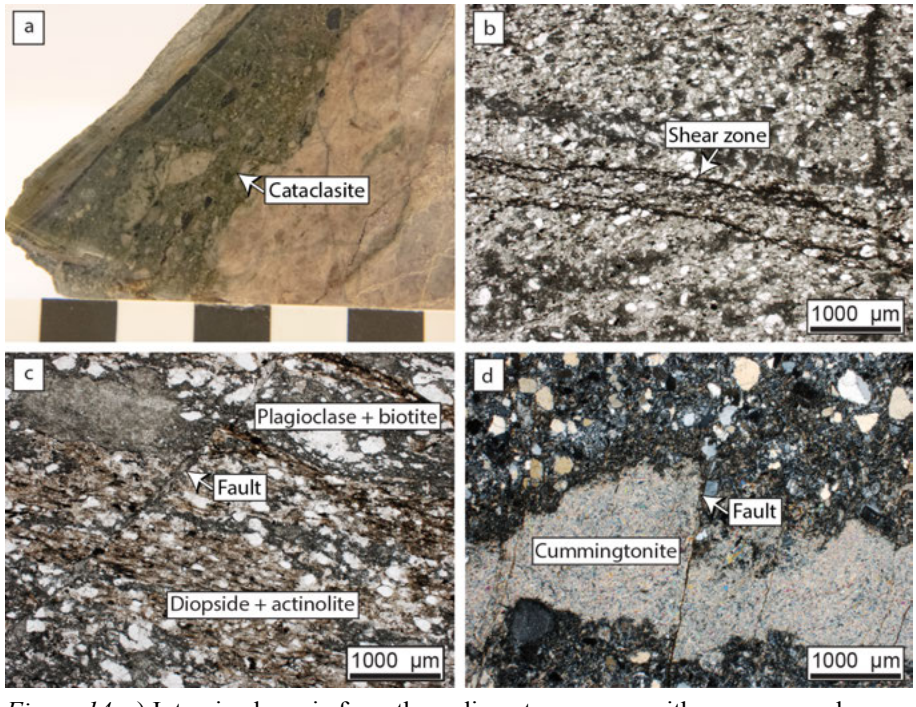

Figure 14. a) Intrusive breccia from the sedimentary screen with green groundmass, feldspar (light), and biotite-rich hornfels (dark) clasts. Fields on the scale are 1 cm long. b) Cataclastic shear zone in hornfels from about 770 m from the granite-greywacke contact (PPL thin section microphotograph). The groundmass in the lighter parts consist of diopside and actinolite, while the groundmass in the darker parts consist of clotted quartz, biotite, and plagioclase. c) Layered groundmass in sample collected about 500 m from the granite contact (PPL thin section microphotograph). The lighter layers consist of diopside and actinolite, while the darker layers consist of clotted quartz, biotite, and plagioclase. A fault with actinolite in the fault plane displaces the altered groundmass. d) Cummingtonite vein in gritstone in a sample collected 70 m from the granite-greywacke contact (CPL thin section microphotograph). The vein is displaced by small faults. The displacement of contact-metamorphic segregations indicates that the emplacement of the granite initially only caused alteration of the rock, while later emplacement also deformed the host rock.

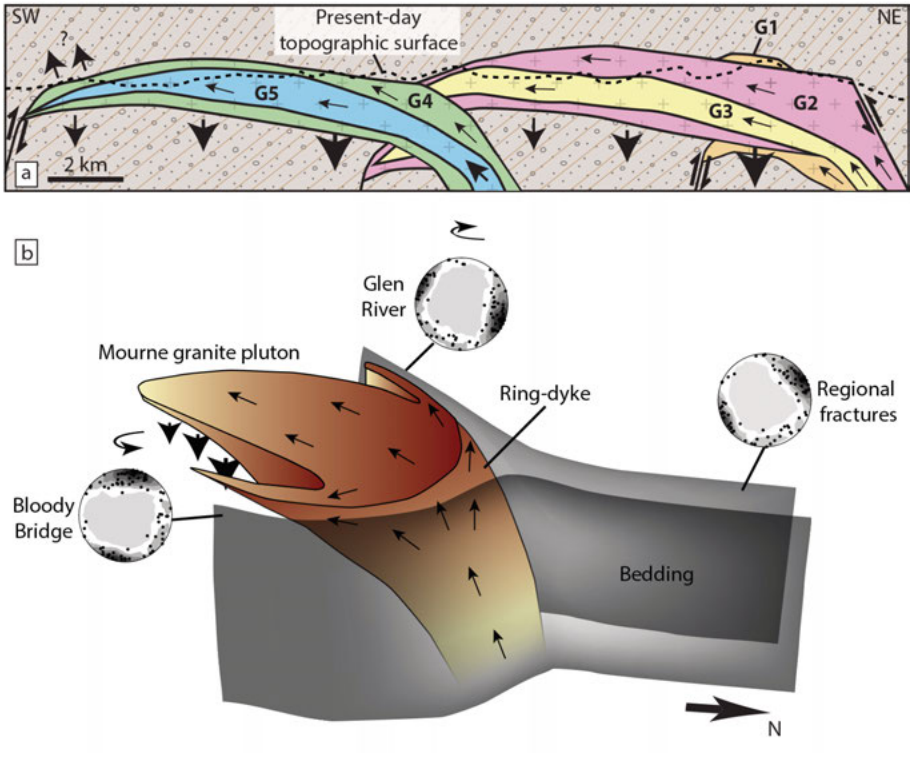

Figure 15. a) Schematic cross-section of the proposed emplacement model of the Mourne granite pluton. The semi-circular north-eastern contact to the pluton and the recorded deformation in the host rock in the NE suggest that the granites G1 - G3 were fed from a ring-dyke and flowed laterally towards the SW (cf. Stevenson *et al.*, 2007). The smaller black arrows indicate magma flow and the larger arrows indicate the displacement of the host rock. The pluton floor is not exposed in the Mourne Mountains; therefore, the pluton may be thicker than indicated in the sketch. b) Schematic sketch of granite emplacement along the north-eastern contact of the Mourne granite pluton. The observed rotation of the host rock and the regional fractures at the north-eastern contact are proposed to be caused by a laterally propagating ring-dyke that also fed the intrusion. The rotation is indicated by the stereonet plots, which show rotated fracture sets in the wall rock to the Mourne granite pluton.

4.3. Paper III

Multi-stage growth of the Cerro Bayo cryptodome, Chachahuén volcano, Argentina – implications for viscous magma emplacement

Cryptodome and dome collapse is associated with volcanic hazards, such as, explosive eruptions, pyroclastic flows, and volcanic edifice collapse (cf. Lipman *et al.*, 1981; Donnadieu *et al.*, 2001). Studying the growth and evolution of volcanic domes provides vital information on the link between

dome growth and the development of weakness zones that may cause collapse.

Following a caldera collapse at 7.1 ± 0.4 Ma (K/Ar, Pérez and Condat, 1996), the Miocene, back-arc Chachahuén volcano entered an edifice rebuilding stage that was characterised by dome and cryptodome growth, as well the deposition of voluminous block and ash flows (see Section 2.3; Palma *et al.*, submitted). We investigated the emplacement of the Cerro Bayo cryptodome using structural mapping, photogrammetry, 3D structural modelling and measurement of magma flow indicators, brittle deformation features and magnetic fabrics with anisotropy of magnetic susceptibility (AMS) from Cerro Bayo with the aim to identify structures and stages of growth.

No chill zones or lithological contacts have been observed in Cerro Bayo, indicating that it grew in a single intrusive event. Magma flow fabrics near the margin of the cryptodome are concentric and indicate contact-parallel flow and internal inflation of the body. Brecciated and fractured portions of Cerro Bayo and complex magmatic and magnetic fabrics in the interior of the cryptodome outline several structural domains (Figure 16a). These domains are separated by moderately to steeply-dipping magmatic shear zones that accommodated intrusion growth and locally overprint the earlier formed concentric fabric (Figure 16b). The nature of the structural domains shows that the emplacement of Cerro Bayo occurred in three stages that resemble the endogenous to exogenous growth of volcanic domes. Cryptodome growth was partly controlled by host-rock deformation, but mainly by magma rheology. The formation of magmatic shear zones during cryptodome growth may have a profound effect on cryptodome stability by creating weakness zones that increase the risk of collapse.

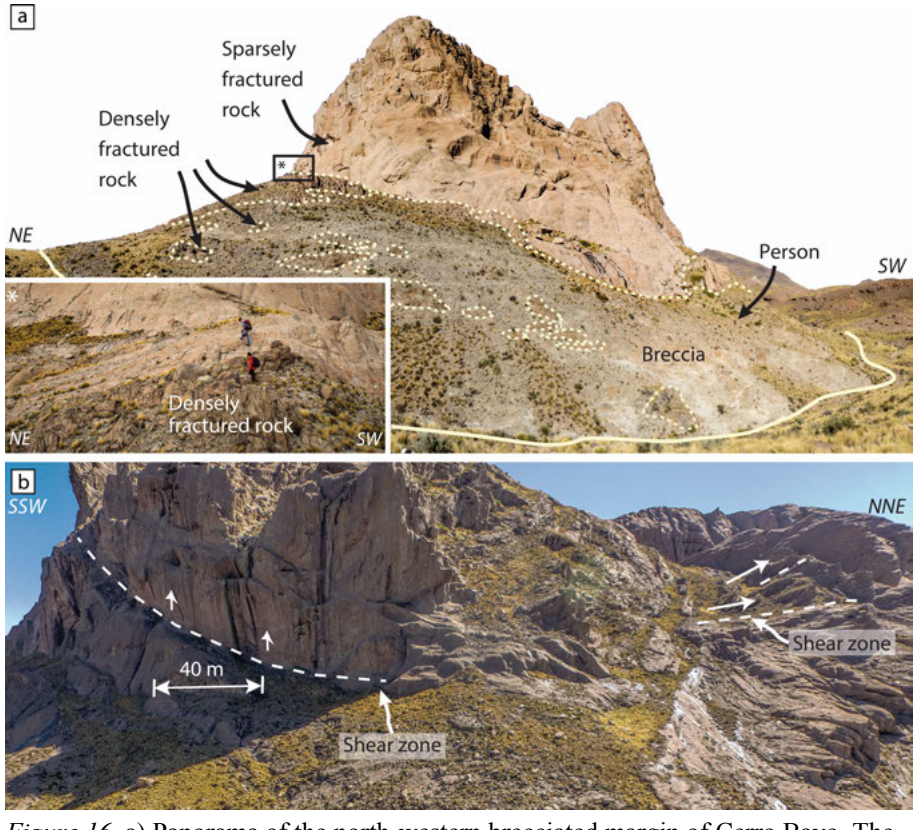

Figure 16. a) Panorama of the north-western brecciated margin of Cerro Bayo. The thickness of the breccia at the location of the photograph is approximately 120 m. Lenses of densely fractured rock occur in the breccia and close to the sparsely fractured intrusion interior. Person for scale is marked with an arrow. Contact between the cryptodome and the host rock is marked by a solid line. The transition between differently fractured units is marked by dotted lines. Inset shows the transition between the sparsely fractured intrusion interior and the densely fractured and brecciated outer part. See people for scale. b) UAS photograph looking west onto the southern ridge of Cerro Bayo. A shear zone (in the right-hand side of the photograph) follows the margin of the ridge. Arrows mark the flow direction of the magma.

4.4. Paper IV

Quantifying the crystal cargo of the Cerro Bayo cryptodome, Argentina; A window into pre-emplacement magma processes and storage conditions

The Cerro Bayo cryptodome was emplaced in the upper kilometre of the Chachahuén volcano at 6.7 ± 0.3 Ma (K/Ar, Pérez and Condat, 1996; see Section 2.3). The growth and shape of cryptodomes are to some degree con-

trolled by viscosity changes in the magma during emplacement (**Papers I and III**). To constrain the characteristics of the Cerro Bayo crypotodome magma prior to emplacement, such as the crystal content of the magma, we investigate pre-emplacement processes in the underlying magma plumbing system using whole rock and mineral major element geochemistry, petrography and crystal size distribution. We also employ amphibole and clinopyroxene-melt thermobarometry to study the architecture of the plumbing system to Cerro Bayo.

Cerro Bayo is composed of a porphyritic trachyandesite and contains numerous mafic enclaves. The main antecrysts/phenocrysts in Cerro Bayo are plagioclase and amphibole and constitute about 30 vol. % of the rock. Minor mineral phases include pyroxene, apatite and magnetite. Several crystal populations with different growth histories were identified in Cerro Bayo. For example, some plagioclase crystals are resorbed and show zones with sharp increase in An mol% (up to 25 %), which indicates recharge of hot relatively mafic magma, while other crystals only record small temperature shifts, likely induced by latent heat of crystallisation (cf. Blundy *et al.*, 2006; Ruprecht and Wörner, 2007; Streck, 2008). Amphibole and clinopyroxene barometers yield average crystallisation pressures that range from 740 to 1036 MPa and reveal a storage region at about 30 to 40 km depth in the lower crust. The voluminous crystal cargo, diverse zoning patterns, sieve-textured plagioclase, and abundant enclaves in Cerro Bayo suggest that the magma was derived from a crystal mush storage region that was mobilised by the recharge of mafic melt.

When the particle fraction exceeds 40 vol. % in a magma, the viscosity increases sharply with further crystallisation (cf. Costa, 2005; Petford, 2009). The voluminous crystal cargo in Cerro Bayo (30 vol. %) suggest that the magma viscosity would have increased rapidly at the onset of groundmass crystallisation and so likely affected the emplacement of the Cerro Bayo cryptodome.

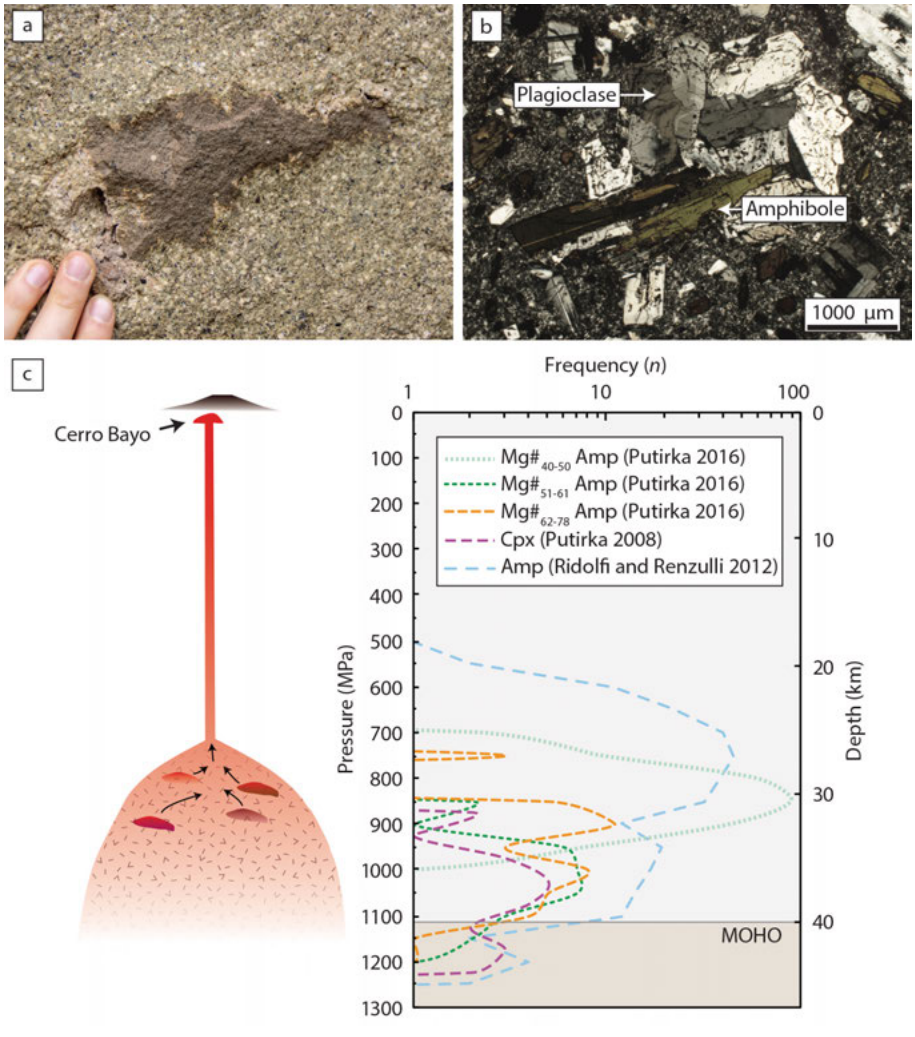

Figure 17. a) Relatively fine-grained dark enclave with cuspate sinusoidal margins in plagioclase- (light mineral) and amphibole- (dark mineral) phyric Cerro Bayo trachyandesite. b) Glomerocryst consisting of plagioclase and amphibole in Cerro Bayo trachyandesite. Note the oscillatory zoning in the plagioclase (CPL thin section). c) Conceptual sketch of the Cerro Bayo plumbing system (left) and the frequency of calculated crystallisation pressures for the different thermobarometric models (right). The barometers indicate magma a storage region in the lower crust. The Cerro Bayo magma is composed of crystals derived from different melt pockets that mixed and ascended in a ~30 km long conduit to Cerro Bayo.

4.5. Paper V

Magma plumbing for the 2014-2015 Holuhraun eruption, Iceland

The eruption at the Holuhraun volcanic fissure between August 2014 and February 2015 was preceded by a propagating seismic swarm and accompanied by subsidence in the Bárðarbunga central volcano caldera approximately 45 km SW of the eruption site throughout the eruption (Sigmundsson *et al.*, 2015; Gudmundsson *et al.*, 2016). However, since the eruption occurred in the neighbouring Askja volcanic swarm there was a need to investigate the source of the erupted products. Samples were collected in September 2014 from lava erupted during the initial stages of the eruption and were analysed for whole rock major, trace elements and oxygen isotopes. We also performed thermobarometry on the eruptive products using major element composition of minerals and whole-rock compositions of the lava.

The lava samples in the study are basaltic, porphyritic, and vesicular. The groundmass contains microlites of plagioclase, clinopyroxene, olivine, and skeletal titanomagnetite. The larger crystals in the samples comprise acicular plagioclase, subhedral clinopyroxene, and subhedral olivine, which occur frequently as aggregates (glomerocrysts). Plagioclase is also present in centimetre-sized gabbro fragments that contain minor olivine. On the basis of major and trace element geochemistry, a compositional affinity between the 2014-15 Holuhraun lavas and the Bárðarbunga-Veiðivötn system is apparent, but the erupted products are distinct from the historical eruption products of the nearby Askja system (Figure 18b). The lava from the Holuhraun eruption shows $\delta^{18}O$ values between 4.4 and 5.4 ‰ (avg. = 5.0 ‰). The gabbro fragments yield a $\delta^{18}O$ range of 4.0 to 5.0 ‰ (avg. = 4.5 ‰) and thus record a slightly lower range than the lava whole rock samples. Clinopyroxene-melt equilibrium thermobarometry resulted in crystallisation pressures between 26 MPa and 882 MPa, with an average of 471 MPa. Assuming an average crustal density of 2700 kg m^{-3}, which corresponds to a depth range of 0.97 to 33 km (avg. ~ 17 km) with corresponding temperatures of 1152 to 1238 °C (avg. 1193°C). Plagioclase-melt thermobarometry resulted in crystallisation pressures between 103 MPa and 165 MPa (avg. ~ 141 MPa), which calculates to 3.8 to 6.1 km depth (avg. ~ 5.2 km). The thermobarometry displays a mid-crustal origin for the clinopyroxene phenocrysts, while plagioclase has distinctly shallower crystallisation depths in the Icelandic upper crust corresponding to the approximate depth of the inferred shallow source magma chamber associated with the caldera unrest (cf. Gudmundsson *et al.*, 2016). The petrological evidence implies that the lavas were derived from a complex and interconnected magma plumbing system spanning between 28 and 5 km depth beneath the Bárðarbunga central volcano wherein discrete magma batches interacted and mixed. Magma initially pooled around 17 to 20 km depth, then it ascended and was temporarily stored at high crustal levels (Figure 18a). There, the magma interacted with, and entrained, gabbro fragments and crystals that are

characterised by resorption, disintegration textures, and $\delta^{18}O$ values lower than MORB. The magma was then laterally transported away from the shallow parts of the Bárðarbunga plumbing system first via a radial dyke and then via a regional dyke until the magma eventually broke through to the surface at the Holuhraun eruption site (Sigmundsson *et al.*, 2015; Gudmundsson *et al.*, 2016).

Figure 18. (Next page). a) Clinopyroxene and plagioclase-melt thermobarometry on the Holuhraun lava show main crystallisation levels at ~ 17 km and ~ 5 km depth, respectively. b) Major element variation diagram of historical basaltic eruptions from the Askja and Bárðarbunga-Veiðivötn volcanic systems (Hartley and Thordarson, 2013). CaO/K_2O ratios in Bárðarbunga-Veiðivötn and recent Holuhraun samples exceed the respective ratios of the Askja eruptive products.

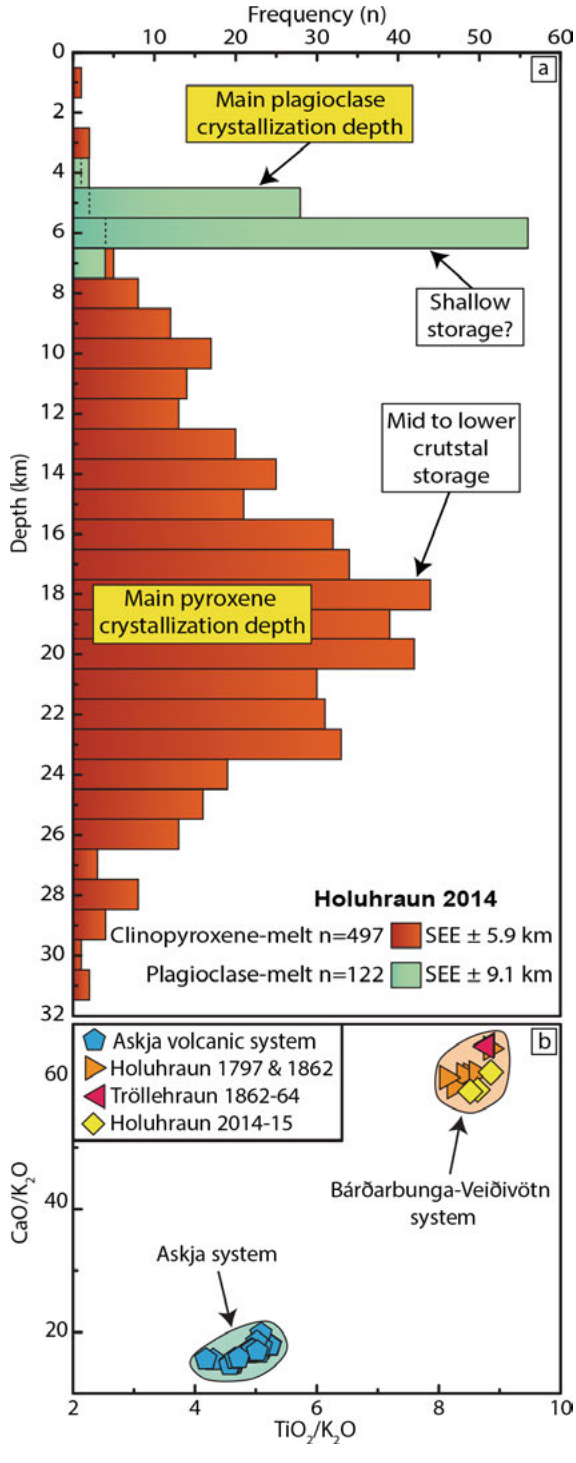
Frequency (n)
10
20
30
40
50
60
a
Main plagioclase crystallization depth
Shallow storage?
Mid to lower crutstal storage
Main pyroxene crystallization depth
Depth (km)
0
2
4
6
8
10
12
14
16
18
20
22
24
26
28
30
32
Holuhraun 2014
Clinopyroxene-melt n=497
SEE ± 5.9 km
Plagioclase-melt n=122
SEE ± 9.1 km
b
Askja volcanic system
Holuhraun 1797 & 1862
Tröllehraun 1862-64
Holuhraun 2014-15
Bárðarbunga-Veiðivötn system
Askja system
CaO/K2O
60
40
20
2
4
6
8
10
TiO2/K2O

5. Conclusions and Outlook

The main focus of this thesis is to investigate different aspects of the emplacement of felsic magma in the shallow crust. Below follow the conclusions of the respective papers and suggestions for future directions of study.

Papers I and III: The Sandfell laccolith and the Cerro Bayo cryptodome both grew in a single intrusive event and record (i) initial inflation that produced contact-parallel magma flow indicators. (ii) Viscous stalling of the rim of the intrusion as an effect of brittle magma deformation, and (iii) subsequent vertical growth as the continuously intruding magma punched through the viscously stalled rim of the intrusions (Figure 19). Our observations show that magma experiences changes in rheology and viscosity during intrusion growth and emplacement, likely caused by strain-induced crystallisation and degassing. These changes in magma viscosity force the intrusion to grow vertically, which creates shear zones and faults within the magma body. However, more efforts are needed to understand the degassing behaviour of the magma during intrusion emplacement, but also how the magma influx rate and conduit processes may affect rheology changes in the magma during cryptodome growth. If fracture band formation is associated with the release of seismic energy, the abundant syn-emplacement fracturing in the Sandfell laccolith also offer an intriguing possibility to study the active growth of similar cryptodomes (given the occasion). The fracture-banded volume (about one third of the intrusion volume) also shows that similar intrusions may be very permeable and could therefore be a good target for geothermal exploration.

Paper II: Of the two contrasting theories of emplacement of the Mourne granite pluton, laccolith vs. cauldron subsidence can neither explain the lack of rotation of the roof of the pluton nor the contact-strike parallel rotation of the wall of the intrusion. Moreover, the displacement and shearing of metamorphic segregations show that contact metamorphism to some extent predated the deformation related to granite emplacement. These observations suggest that initial granite emplacement did not cause any observable deformation of the roof and wall rock, while later intrusion involved deformation. The aureole therefore provides evidence of different types of emplacement mechanisms for the Mourne pluton granite magma. A model involving both floor subsidence and host rock uplift and deflection is presented based on both our data and the findings of previous investigations. The Mourne Mountains granite pluton highlights the complex deformation patterns that

might be associated with the emplacement of large amounts of felsic magma close to the surface.

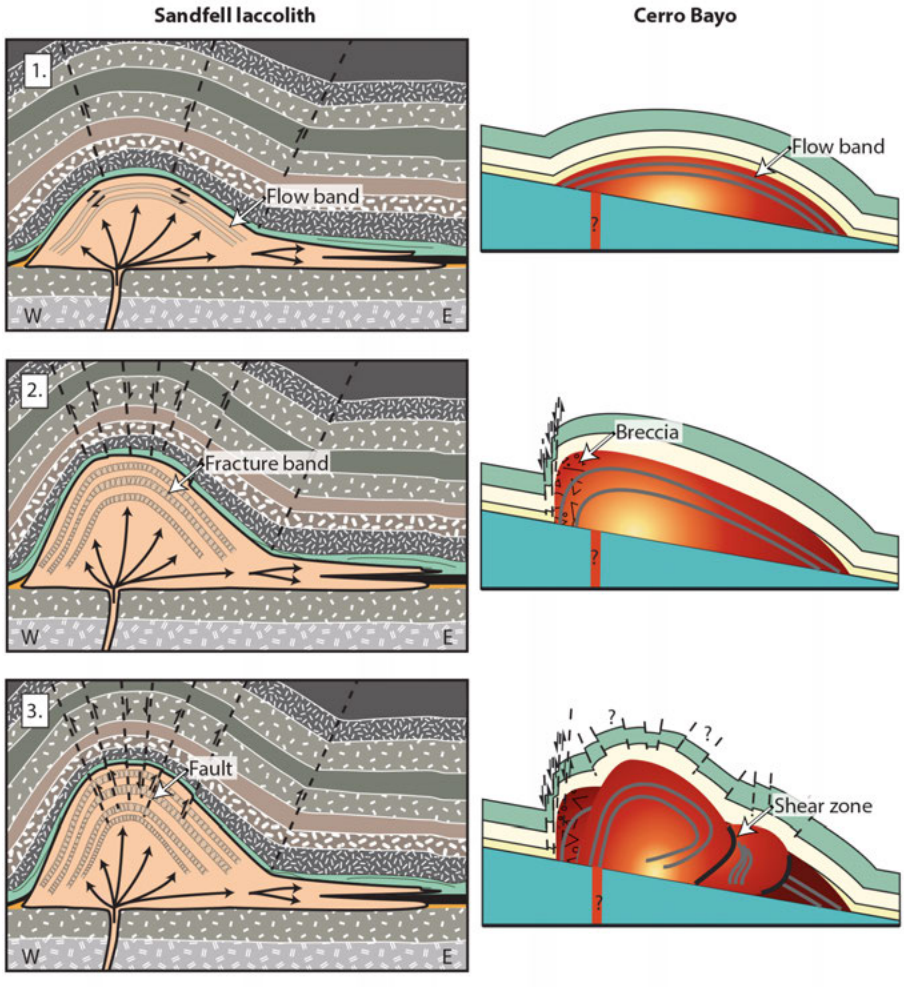

Figure 19. The different growth stages of the Sandfell laccolith and the Cerro Bayo cryptodome. See text for details.

Paper IV: The Cerro Bayo magma was generated in a crystal mush-system in the lower crust. Abundant magmatic enclaves and reverse crystal zoning patterns show that mobilisation of the crystal mush was likely associated with the recharge of hotter, compositionally different magma. The Cerro Bayo magma carried about 30 vol. % of crystal cargo from the deep storage into the cryptodome. This has large implications for magma rheology and likely affected the growth of the cryptodome by controlling the transition between different growth stages. However, a more detailed study of the groundmass microlites from different structural domains in the Cerro Bayo

cryptodome needs to be attempted to test if there is any correlation between crystallinity and the growth style.

Paper V highlights the complex tectono-magmatic relationships at active Icelandic volcanoes. Even though the paper only uses geochemistry and petrology, the magmatic event itself shows the importance of multiple approaches to understand the plumbing system to an active volcano. The knowledge we have about this eruptive event today is the result of the combined efforts of many researches from different fields of magma plumbing research. While geochemistry constrained reservoir depths and source, geophysical and geodetic methods resolved the transport.

This thesis shows that felsic magma emplacement in the upper crust is dynamic and involves multiple mechanisms that affect the growth and shape of the intrusions. An integrated approach considering both the magma rheology and the host rock is therefore needed to fully understand the shallow magma plumbing system and its effect on volcanism.

6. Summary in Swedish

Denna avhandling handlar om hur granitiska magmakammare bildas i det magmatiska systemet i den övre jordskorpan. Det magmatiska systemet definieras som en magmas transportkanaler och förvaringsområden under vulkanen. Processerna i det magmatiska systemet och hur det är uppbyggt påverkar vulkanens karaktär, till exempel om ett utbrott blir explosivt eller effusivt (lavaflöde). Den övre skorpan består till stor del av lagrade bergarter av sedimentärt eller magmatiskt ursprung som deformeras sprött, vilket påverkar hur en magmakammare bildas. Tidigare strukturgeologiska studier om hur en magmakammare bildas har främst undersökt hur de omgivande bergarterna påverkas av magmakammaren medans magma antas vara en het högstrycksvätska. Petrologer som forskar om bergartsbildning ser en magmakammare som en reservoar bestående främst av kristaller. Personer som studerar vulkaner undersöker hur en magmas skiftande egenskaper påverkar vulkanutbrottets karaktär. De varierande definitionerna av magma och det magmatiska systemet visar att det behövs en enhetlig sammanbindande syn på hur det magmatiska systemet fungerar. Denna avhandling undersöker både den omgivande bergarten och magman i magmakammaren för att förstå dynamiken i det magmatiska systemet. Jag studerar processer i stelnade och exponerade magmakammare som var aktiva för flera miljoner år sedan för att förstå processer i aktiva magmakammare idag.

Artikel I och III undersöker hur lakkoliter och så kallade cryptodomer växer. En lakkolit eller en cryptodom är en kupolformad magmakammare med platt golv. **Artikel I** handlar om den ryolitiska Sandfell-lakkoliten på östra Island som bildades för ungefär 11,7 miljoner år sedan. Sandfell-lakkoliten bildades på ett djup av 540 meter genom att magman lyfte upp och trycka iväg det omgivande berget. I studien undersöktes magmaflödet i magmakammaren genom att mäta flödesstrukturer i fält och mineralorientering med hjälp av AMS (anisotropy of magnetic susceptibility). Flödesmönstret visar att magman som flödade in i Sandfell kontinuerligt deformerade tidigare inflöden magma. Detta fragmenterade stora delar av Sandfell-lakkoliten, det vill säga att magman stelnade samtidigt som lakkoliten växte. **Artikel III** fokuserar på Cerro Bayo-cryptdomen i Argentina. Cerro Bayo bildades för 6.7 miljoner år sedan och har en trachyandesitisk kemisk sammansättning. Magmatiska flödesstrukturer är parallella med kontakten mellan Cerro Bayo och det omgivande berget, men nästan vertikala i mitten av cryptodomen. Längs Cerro Bayos västra kontakt finns en breccia. Flö-

desmönstren och fördelningen av sprickor i Cerro Bayo visar att den växte initialt likt en ballong. Men när magman närmast kontakten stelnade på grund av deformation, tvingade den Cerro Bayo att växa på höjden längs nästan vertikala skjuvzoner i magman. Studierna visar att reologiändringar i magman (som beror på dess viskositet och andelen kristaller) som sker samtidigt som lakkoliten bildas tvingar den att växa på höjden vilket skapar dess karakteristiska kupolform.

Artikel II undersöker hur den granitiska magmakammaren i Mournebergen i Nordirland bildades. Två rakt motstående teorier har tidigare framförts. Den första teorin föreslår att magmakammaren bildades genom att kammargolvet sjönk och skapade utrymme för magman. Det betyder att magmakammarens tak inte ska ha blivit deformerat. Den andra teorin antar att magmakammaren har bildats som en lakkolit som tryckt iväg och deformerat taket till magmakammaren. I artikeln testas de två teorierna genom att mäta regionala sprickmönster i den omgivande bergarten och genom att studera kontakmetamorfos. Kontaktmetamorfos är de omvandlingar som sker i det omgivande berget runt en magmakammare till följd av värmetillförsel från magman och genom transport av reaktiva fluider i berggrunden. Sprickmönstren är väldigt lika i taket runt om magmakammaren vilket indikerar att det inte uppdämts av magma. Väggen till magmakammaren är å andra sidan roterad parallell med strykningen av kontakten till magmakammaren. Kontatkmetamorfosen visar att det omgivande berget initialt värmdes upp och i ett senare skede deformerades. Detta indikerar att två eller flera mekanismer skapade plats för granitmagman i den övre skorpan. Vi föreslår att magmakammaren inledningsvis bildades genom att golvet sjönk som en fallucka vilket senare deformerade väggen men inte taket till magmakammaren.

Artikel IV undersöks det magmatiska systemet till Cerro Bayo med termobarometri och kristallstorleksfördelning (crystal size distribution). Cerro Bayos magma innehåller ungefär 30 vol. % av plagioklas och amfibol som kristalliserade innan magman trängde in i den övre skorpan och bildade Cerro Bayo. Det finns också flera magmatiska enklaver av mafisk kemisk sammansättning i Cerro Bayo. Termobarometri visar att amfibol kristalliserade på ett djup av 30 till 40 km i den undre skorpan. Det som remobiliserade den kristallrika magman var tillförseln av mer mafisk magma vilket växtzoner i kristallerna visar. Den höga kristallhalten betyder att allteftersom magman kristalliserade ökade viskositeten på magman snabbt, vilket troligtvis påverkade hur Cerro Bayo-cryptodomen växte genom att ändra magmareologin.

Artikel V handlar om Holuhraunutbrottet 2014–2015 i Island. Före utbrottet rörde sig en jordbävningssvärm från vulkanen Bárðarbunga till utbrottsplatsen och under hela vulkanutbrottet bildades sättningar i Bárðarbunga vulkanen. Lava från utbrottet studerades med termobarometri och geokemi för att förstå hur det magmatiska systemet till vulkanen var uppbyggt. Vårt data visar att pyroxen kristalliserade i den mellersta skorpan

medans plagioklas kristalliserade i en grundare magmakammare. Kemiskt sett är Holuhraunlavan lik tidigare utbrott i Bárðarbungasystemet. Tillsammans med geofysiska data tyder våra observationer på att utbrottet har sitt ursprung i ett vertikalt extensivt magmatiskt system under Bárðarbunga och transporterades i en magmatisk gång till utbrottsplatsen.

Studierna i denna avhandling visar att för att förstå hur magmakammare bildas och det magmatiska systemet, krävs integrerade studier som tar hänsyn till både magman och de omgivande bergarterna.

7. Acknowledgements

Steffi, thank you for taking me along on the journey through the magma plumbing system, your support throughout my Ph. D. studies and teaching me the art of "walking with the scree". Of all the types of scree that I have walked on, I will most cherish our days on the slopes of Sandfell, which in my opinion has the best scree in the world. I would also like to thank my other supervisor Karen for stimulating and interesting discussions. Your company in the field in the Mourne Mountains made the extremely rainy days enjoyable.

Val, thank you for introducing me to the British and Irish Palaeogene Igneous province and your help before and during my Ph. D. studies. Frances, thank you for the help during the first part of my Ph. D. studies and company in the Mourne Mountains and on Gran Canaria.

I would like to thank the Ph. D. students in the MPT group that have come and gone during the years Börje, Sylvia, Dave, Lukas, Kirsten, Hong Ling, Franz, Iwona, Lei, Hoachen and Thorben for useful discussions and assistance when needed. Especially my office mates during different parts of my Ph. D., Harri, Erika and Emma for rewarding discussions. For example, the discussion with Erika about honouring deadlines. I now also swear fluently in Italian. Emma, thank you for your help proof-reading the thesis. Harri, thanks for your company during field work. I will always remember the crazy roads that our car was not built for and the ticks on Gran Canaria. I would like to thank the senior staff in the MPT group Håkan, Örjan, Peter, Hannes, Hans, Karin, Jarek and Abi for company during teaching in the field and interesting discussions. I am grateful to the Oslo group Olivier, Frank, Tobias, Øysten, Ben, Håvard, Alban, Ole, for stimulating scientific discussion and for making my stays in Oslo and the conferences we attended together very pleasant. I like to thank the students I worked together with on some projects for assistance in the field and help in the lab, Adam, Maria, Yang, Weronika, Elin and Marcus. Geologi-gänget Tomas, Adrian, Franz, Johan, and Per, we have had some very funny trips that helped me forget about the thesis for a bit. I hope there will be another one soon.

Bjarne, thank you for introducing me to AMS and the interesting discussions about magmatic fabrics and Olafúr for discussions about Iceland and seismicity related to magmatic and volcanic activity.

I like to thank the participants of the Wednesday magma meeting group especially Chris, Rémi, Mohsen (Måsen) for making me think about the physics of magma flow.

I would like to thank all the co-authors on the papers for valuable input and assistance in completing the thesis.

I am grateful to Midland Valley Ltd. and PETEX for providing an academic license to MOVE™ and to Uni Research CIPR, University of Bergen for making LIME free to use. I would also thank the scholarship foundations that have funded several of my field campaigns, Otterborgs, Jänes, Uddeholms, Mourne-Cooley-Gullion, KVA Geoscience, Linnéstiftelsen. Without the funding, several of the papers in the thesis would not have been written.

I would lastly like to thank my family for the support and help during my Ph. D. studies and especially in the final weeks before the thesis deadline. I really don't know why we decided to renovate the kitchen at the same time as the thesis deadline. Thanks to Pontus for letting me stay with him while visiting the University of Oslo. Finally, Hanna thank you for your company throughout my studies and bearing with me during these final months of the thesis write-up!

8. References

Akiman, O. (1971). The petrology and geochemistry of the tertiary dyke swarm associated with the Mourne mountian granites, Northern Ireland. Doctoral dissertation, Univeristy of Durham, Durham.

Allmendinger, R. W., Cardozo, N. & Fisher, D. (2012). *Structural Geology Algorithms: Vectors and Tensors*. Cambridge: Cambridge University Press.

Allmendinger, R. W., Siron, C. R. & Scott, C. P. (2017). Structural data collection with mobile devices: Accuracy, redundancy, and best practices. *Journal of Structural Geology* **102**, 98–112.

Anderson, E. M. (1937). IX.—The Dynamics of the Formation of Cone-sheets, Ring-dykes, and Caldron-subsidences. *Proceedings of the Royal Society of Edinburgh* **56**, 128–157.

Anderson, P. E., Stevenson, C. T., Cooper, M. R., Meighan, I. G., Reavy, R. J., Hurley, C. T., Inman, J. & Ellam, R. M. (2017). Refined model of incremental emplacement based on structural evidence from the granodioritic Newry igneous complex, Northern Ireland. *GSA Bulletin*.

Anderson, T. B. (1987). The onset and timing of Caledonian sinistral shear in County Down. *Journal of the Geological Society, London* **144**, 817–825.

Anderson, T. B. (2000). Structural interpretations of the Southern Uplands Terrane. *Transactions of the Royal Society of Edinburgh: Earth Sciences* **91**, 363–373.

Anderson, T. B. (2004). Southern Uplands-Down-Longford Terrane. In: Mitchell, W. I. (ed.) *The geology of Northern Ireland: Our Natural Foundation*. Belfast: Geological Survey of Northern Ireland, 41–60.

Anderson, T. B. & Cameron, T. D. J. (1979). A structural profile of Caledonian deformation in Down. *Geological Society, London, Special Publications* **8**, 263–267.

Bailey, E. B., Clough, C. T., Wright, W. B., Richey, J. E. & Wilson, G. V. (1924). *The Tertiary and Post-Tertiary Geology of Mull, Loch Aline and Oban*. Edinburgh: Memoir of the Geological Survey of Great Britain, Sheet 44 (Scotland), HMSO.

Baker, D. R., Mancini, L., Polacci, M., Higgins, M. D., Gualda, G. A. R., Hill, R. J. & Rivers, M. L. (2012). An introduction to the application of X-ray microtomography to the three-dimensional study of igneous rocks. *Lithos* **148**, 262–276.

Bell, B. R. & Williamson, I. T. (2002). Tertiary igneous activity. In: Trewin, N. H. (ed.) *The Geology of Scotland*. Oxford: The Geological Society London, 371–407.

Bemis, S. P., Micklethwaite, S., Turner, D., James, M. R., Akciz, S., Thiele, S. T. & Bangash, H. A. (2014). Ground-based and UAV-Based photogrammetry: A multi-scale, high-resolution mapping tool for structural geology and paleoseismology. *Journal of Structural Geology* **69**, 163–178.

Benn, K. & Allard, B. (1989). Preferred Mineral Orientations Related to Magmatic Flow in Ophiolite Layered Gabbros. *Journal of Petrology* **30**, 925–946.

Berg, S. E., Troll, V. R., Harris, C., Deegan, F. M., Riishuus, M. S., Burchardt, S. & Krumbholz, M. (2018). Exceptionally high whole-rock δ18O values in intra-caldera rhyolites from Northeast Iceland. *Mineralogical Magazine* 1–37.

Blundy, J., Cashman, K. & Humphreys, M. (2006). Magma heating by decompression-driven crystallization beneath andesite volcanoes. *Nature* **443**, 76–80.

Breitkreuz, C., Ehling, B.-C. & Pastrik, N. (2015). The Subvolcanic Units of the Late Paleozoic Halle Volcanic Complex, Germany: Geometry, Internal Textures and Emplacement Mode. In: Breitkreuz, C. & Rocchi, S. (eds) *Physical Geology of Shallow Magmatic Systems. Advances in Volcanology (An Official Book Series of the International Association of Volcanology and Chemistry of the Earth's Interior)*. Springer, Cham, 295–307.

Bunger, A. P. & Cruden, A. R. (2011). Modeling the growth of laccoliths and large mafic sills: Role of magma body forces. *Journal of Geophysical Research* **116**, B02203.

Burchardt, S. (2018). Introduction to Volcanic and Igneous Plumbing Systems—Developing a Discipline and Common Concepts. In: Burchardt, S. (ed.) *Volcanic and Igneous Plumbing Systems*. Amsterdam: Elsevier, 1–12.

Burchardt, S. & Gudmundsson, A. (2009). The infrastructure of Geitafell volcano, southeast Iceland. *Studies in Volcanology: The Legacy of George Walker, Spec. Publ. of IAVCEI* **2**, 349–370.

Burchardt, S., Tanner, D. & Krumbholz, M. (2012). The Slaufrudalur pluton, southeast Iceland—An example of shallow magma emplacement by coupled cauldron subsidence and magmatic stoping. *Geological Society of America Bulletin* **124**, 213–227.

Carmichael, I. S. E. (1964). The Petrology of Thingmuli, a Tertiary Volcano in Eastern Iceland. *Journal of Petrology* **5**, 435–460.

Cashman, K. & Blundy, J. (2013). Petrological cannibalism: the chemical and textural consequences of incremental magma body growth. *Contributions to Mineralogy and Petrology* **166**, 703–729.

Cashman, K. V., Sparks, R. S. J. & Blundy, J. D. (2017). Vertically extensive and unstable magmatic systems: A unified view of igneous processes. *Science* **355**, eaag3055.

Cashman, K. V (1990). Textural constraints on the kinetics of crystallization of igneous rocks. *Reviews in Mineralogy and Geochemistry* **24**, 259–314.

Cashman, K. V & Marsh, B. D. (1988). Crystal size distribution (CSD) in rocks and the kinetics and dynamics of crystallization II: Makaopuhi lava lake. *Contributions to Mineralogy and Petrology* **99**, 292–305.

Cassidy, M., Manga, M., Cashman, K. & Bachmann, O. (2018). Controls on explosive-effusive volcanic eruption styles. *Nature Communications* **9**, 2839.

Castro, J. M., Cordonnier, B., Schipper, C. I., Tuffen, H., Baumann, T. S. & Feisel, Y. (2016). Rapid laccolith intrusion driven by explosive volcanic eruption. *Nature Communications* **7**, 13585.

Castro, J. M., Dingwell, D. B., Nichols, A. R. L. & Gardner, J. E. (2005). New insights on the origin of flow bands in obsidian. In: Manga, M. & Ventura, G. (eds) *Special Paper 396: Kinematics and dynamics of lava flows*. Boulder, Colorado: Geological Society of America, 55–65.

Clough, C. T., Maufe, H. B. & Bailey, E. B. (1909). The Cauldron-Subsidence of Glen Coe, and the Associated Igneous Phenomena. *Quarterly Journal of the Geological Society* **65**, 611–678.

Cooper, M. R., Anderson, H., Walsh, J. J., Van Dam, C. L., Young, M. E., Earls, G. & Walker, A. (2012). Palaeogene Alpine tectonics and Icelandic plume-related magmatism and deformation in Northern Ireland. *Journal of the Geological Society* **169**, 29–36.

Cooper, M. R. & Johnston, T. P. (2004). Palaeogene intrusive rocks. In: Mitchell, W. I. (ed.) *The geology of Northern Ireland: Our Natural Foundation*. Belfast: Geological Survey of Northern Ireland, 179–198.

Corry, C. E. (1988). Laccoliths; Mechanics of emplacement and growth. *GSA Special Papers* **220**, 1–114.

Costa, A. (2005). Viscosity of high crystal content melts: Dependence on solid fraction. *Geophysical Research Letters* **32**, L22308.

Cruden, A. R. (1998). On the emplacement of tabular granites. *Journal of the Geological Society* **155**, 853–862.

Cruden, A. R. & McCaffrey, K. J. W. (2001). Growth of plutons by floor subsidence: implications for rates of emplacement, intrusion spacing and melt-extraction mechanisms. *Physics and Chemistry of the Earth, Part A: Solid Earth and Geodesy* **26**, 303–315.

de Saint-Blanquat, M., Habert, G., Horsman, E., Morgan, S. S., Tikoff, B., Launeau, P. & Gleizes, G. (2006). Mechanisms and duration of non-tectonically assisted magma emplacement in the upper crust: The Black Mesa pluton, Henry Mountains, Utah. *Tectonophysics* **428**, 1–31.

Donnadieu, F., Merle, O. & Besson, J.-C. (2001). Volcanic edifice stability during cryptodome intrusion. *Bulletin of Volcanology* **63**, 61–72.

Einarsson, T. (1991). Myndun og mótun lands. *Mál of Menning*. Reykjavik.

Emeleus, C. H. (1955). The granites of the western Mourne Mountains, County Down. *The Scientific Proceedings of the Royal Dublin Society* **27**, 35–52.

Emeleus, C. H. & Bell, B. R. (2005). *British Regional Geology: the Palaeogene Volcanic Districts of Scotland*. Nottingham: British Geological Survey.

Eriksson, P. I., Riishuus, M. S., Sigmundsson, F. & Elming, S.-Å. (2011). Magma flow directions inferred from field evidence and magnetic fabric studies of the Streitishvarf composite dike in east Iceland. *Journal of Volcanology and Geothermal Research* **206**, 30–45.

Fisher, N. I., Lewis, T. & Embleton, B. J. J. (1993). *Statistical Analysis of Spherical Data*. Cambridge, UK: Cambridge University Press.

Geoffroy, L., Callot, J. P., Aubourg, C. & Moreira, M. (2002). Magnetic and plagioclase linear fabric discrepancy in dykes: a new way to define the flow vector using magnetic foliation. *Terra Nova* **14**, 183–190.

Gibson, D., McCormick, A. G., Meighan, I. G. & Halliday, A. N. (1987). The British Tertiary Igneous Province: Young Rb-Sr Ages for the Mourne Mountains Granites. *Scottish Journal of Geology* **23**, 221–225.

Gibson, I. L. (1963). The Reydarfjordur acid volcano centre of eastern Iceland. Doctoral dissertation, Imperial college, University of London.

Gibson, I. L., Kinsman, D. J. J. & Walker, G. P. L. (1966). *Geology of the Faskrudsfjördur area, eastern Iceland*. *Greinar*. Reykjavik: Visindafelag Islendiga.

Gilbert, G. K. (1877). *Report on the geology of the Henry Mountains*. US Geographical and Geological Survey, Washington, DC.

Gonnermann, H. M. & Manga, M. (2005). Flow banding in obsidian: A record of evolving textural heterogeneity during magma deformation. *Earth and Planetary Science Letters* **236**, 135–147.

Gonnermann, H. M. & Manga, M. (2013). Dynamics of magma ascent in the volcanic conduit. In: Fagents, S. A., Gregg, T. K. P. & Lopes, R. M. C. (eds) *Modeling Volcanic Processes*. Cambridge: Cambridge University Press, 55–84.

Goto, Y. & McPhie, J. (1998). Endogenous growth of a Miocene submarine dacite cryptodome, Rebun Island, Hokkaido, Japan. *Journal of Volcanology and Geothermal Research* **84**, 273–286.

Goto, Y., Shingo, K., Noriyoshi, T. & Katsuto, N. (2000). Internal Structures and Fracture Networks in a Miocene Dacite Intrusion, Rebun Island, Hokkaido, Japan. *World Geothermal Congress*. International Geothermal Association, R0144.

Gudmundsson, M. T. *et al.* (2016). Gradual caldera collapse at Bárdarbunga volcano, Iceland, regulated by lateral magma outflow. *Science* **353**, aaf8988.

Hartley, M. E. & Thordarson, T. (2013). The 1874-1876 volcano-tectonic episode at Askja, North Iceland: Lateral flow revisited. *Geochemistry, Geophysics, Geosystems* **14**, 2286–2309.

Hawkes, L. & Hawkes, H. K. (1933). The Sandfell Laccolith and 'Dome of Elevation.' *Quarterly Journal of the Geological Society* **89**, 379–400.

Helgason, J. (1984). Frequent shifts of the volcanic zone in Iceland. *Geology* **12**, 212.

Higgins, M. D. (1998). Origin of Anorthosite by Textural Coarsening: Quantitative Measurements of a Natural Sequence of Textural Development. *Journal of Petrology* **39**, 1307–1323.

Higgins, M. D. (2000). Measurement of crystal size distributions. *American Mineralogist* **85**, 1105–1116.

Higgins, M. D. & Roberge, J. (2003). Crystal Size Distribution of Plagioclase and Amphibole from Soufriere Hills Volcano, Montserrat: Evidence for Dynamic Crystallization-Textural Coarsening Cycles. *Journal of Petrology* **44**, 1401–1411.

Holohan, E. P., Troll, V. R., Walter, T. R., Münn, S., McDonnell, S. & Shipton, Z. K. (2005). Elliptical calderas in active tectonic settings: an experimental approach. *Journal of Volcanology and Geothermal Research* **144**, 119–136.

Hood, D. N. (1981). Geochemical, petrological and structural studies on the tertiary granites and associated rocks of the Eastern Mourne Mountains, Co. Down, Northern Ireland. Doctoral dissertation, Queen's University, Belfast.

Hutton, D. H. W. (1988). Granite emplacement mechanisms and tectonic controls: inferences from deformation studies. *Transactions of the Royal Society of Edinburgh: Earth Sciences* **79**, 245–255.

Jackson, M. D. & Pollard, D. D. (1988). The laccolith-stock controversy: New results from the southern Henry Mountains, Utah. *Geological Society of America Bulletin* **100**, 117–139.

Jelínek, V. (1981). Characterization of the magnetic fabric of rocks. *Tectonophysics* **79**, T63–T67.

Jerram, D. A., Cheadle, M. J. & Philpotts, A. R. (2003). Quantifying the Building Blocks of Igneous Rocks: Are Clustered Crystal Frameworks the Foundation? *Journal of Petrology* **44**, 2033–2051.

Jerram, D. A., Dobson, K. J., Morgan, D. J. & Pankhurst, M. J. (2018). The Petrogenesis of Magmatic Systems: Using Igneous Textures to Understand Magmatic Processes. In: Burchardt, S. (ed.) *Volcanic and Igneous Plumbing Systems*. Amsterdam: Elsevier, 191–229.

Jerram, D. A. & Higgins, M. D. (2007). 3D Analysis of Rock Textures: Quantifying Igneous Microstructures. *Elements* **3**, 239–245.

Jerram, D. A., Mock, A., Davis, G. R., Field, M. & Brown, R. J. (2009). 3D crystal size distributions: A case study on quantifying olivine populations in kimberlites. *Lithos* **112**, 223–235.

Jolly, R. J. H. & Sanderson, D. J. (1995). Variation in the form and distribution of dykes in the Mull swarm, Scotland. *Journal of Structural Geology* **17**, 1543–1557.

Kay, S. M., Mancilla, O. & Copeland, P. (2006). Evolution of the late Miocene Chachahuén volcanic complex at 37°S over a transient shallow subduction zone under the Neuquén Andes. In: Kay, S. M. & Ramos, V. (eds) *Special Paper 407: Evolution of an Andean Margin: A Tectonic and Magmatic View from the Andes to the Neuquén Basin (35°-39°S lat)*. Geological Society of America, 215–246.

Kelley, D. F. & Barton, M. (2008). Pressures of Crystallization of Icelandic Magmas. *Journal of Petrology* **49**, 465–492.

Kennedy, B. M., Holohan, E. P., Stix, J., Gravley, D., Davidson, J. P., Cole, J. & Burchardt, S. (2018). Volcanic and Igneous Plumbing Systems of Caldera Volcanoes. In: Burchardt, S. (ed.) *Volcanic and Igneous Plumbing Systems*. Amsterdam: Elsevier, 253–278.

Kennedy, B., Wilcock, J. & Stix, J. (2012). Caldera resurgence during magma replenishment and rejuvenation at Valles and Lake City calderas. *Bulletin of Volcanology* **74**, 1833–1847.

Kerr, A. D. & Pollard, D. D. (1998). Toward more realistic formulations for the analysis of laccoliths. *Journal of Structural Geology*. Pergamon **20**, 1783–1793.

Ketcham, R. A. (2005a). Three-dimensional grain fabric measurements using high-resolution X-ray computed tomography. *Journal of Structural Geology* **27**, 1217–1228.

Ketcham, R. A. (2005b). Computational methods for quantitative analysis of three-dimensional features in geological specimens. *Geosphere* **1**, 32.

Khan, M. A. (1962). The anisotropy of magnetic susceptibility of some igneous and metamorphic rocks. *Journal of Geophysical Research* **67**, 2873–2885.

Larsen, G. & Gudmundsson, M. T. (2016). The Bárðarbunga volcanic system. In: Ilyinskaya, E., Larsen, G. & Gudmundsson, M. T. (eds) *Catalogue of Icelandic Volcanoes*.

Le Bas, M. J. (1971). Per-alkaline Volcanism, Crustal Swelling, and Rifting. *Nature Physical Science* **230**, 85–87.

Lipman, P. W. (1984). The roots of ash flow calderas in western North America: Windows into the tops of granitic batholiths. *Journal of Geophysical Research* **89**, 8801.

Lipman, P. W., Moore, J. G. & Swanson, D. A. (1981). Bulging of the north flank before the May 18 eruption - geodetic data. In: Lipman, P. W. & Mullineaux, D. R. (eds) *The 1980 Eruptions of Mount Saint Helens, Washington. Geol. Surv. Prof. Paper 1250*. Washington, D. C.: United States Government Printing Office, 143–155.

Llambías, E. J., Bertotto, G. W., Risso, C. & Hernando, I. R. (2010). El volcanismo cuaternario en el retroarco de Payenia: una revisión. *Revista de la Asociación Geológica Argentina* **67**, 278–300.

Macdonald, R., Bagiński, B., Upton, B. G. J., Dzierżanowski, P. & Marshall-Roberts, W. (2009). The Palaeogene Eskdalemuir dyke, Scotland: long-distance lateral transport of rhyolitic magma in a mixed-magma intrusion. *Mineralogical Magazine* **73**, 285–300.

Macdonald, R., Fettes, D. J. & Bagiński, B. (2015). The Mull Paleocene dykes: some insights into the nature of major dyke swarms. *Scottish Journal of Geology* **51**, 116–124.

Marsh, B. D. (1988). Crystal size distribution (CSD) in rocks and the kinetics and dynamics of crystallization. *Contributions to Mineralogy and Petrology* **99**, 277–291.

Marsh, B. D. (1998). On the Interpretation of Crystal Size Distributions in Magmatic Systems. *Journal of Petrology* **39**, 553–599.

Martin, E., Paquette, J. L., Bosse, V., Ruffet, G., Tiepolo, M. & Sigmarsson, O. (2011). Geodynamics of rift–plume interaction in Iceland as constrained by new $^{40}Ar/^{39}Ar$ and in situ U–Pb zircon ages. *Earth and Planetary Science Letters* **311**, 28–38.

McCarthy, W., Petronis, M. S., Reavy, R. J. & Stevenson, C. T. (2015). Distinguishing diapirs from inflated plutons: an integrated rock magnetic fabric and structural study on the Roundstone Pluton, western Ireland. *Journal of the Geological Society* **172**, 550–565.

Meighan, I. G., Gibson, D. & Hood, D. N. (1984). Some Aspects of Tertiary Acid Magmatism in NE Ireland. *Mineralogical Magazine* **48**, 351–363.

Menand, T. (2011). Physical controls and depth of emplacement of igneous bodies: A review. *Tectonophysics*. Elsevier **500**, 11–19.

Michel, J., Baumgartner, L., Putlitz, B., Schaltegger, U. & Ovtcharova, M. (2008). Incremental growth of the Patagonian Torres del Paine laccolith over 90 k.y. *Geology* **36**, 459.

Minakami, T., Ishikawa, T. & Yagi, K. (1951). The 1944 Eruption of Volcano Usu in Hokkaido, Japan. *Bulletin Volcanologique* **11**, 45–157.

Mock, A. & Jerram, D. A. (2005). Crystal Size Distributions (CSD) in Three Dimensions: Insights from the 3D Reconstruction of a Highly Porphyritic Rhyolite. *Journal of Petrology* **46**, 1525–1541.

Mock, A., Jerram, D. A. & Breitkreuz, C. (2003). Using Quantitative Textural Analysis to Understand the Emplacement of Shallow-Level Rhyolitic Laccoliths - a Case Study from the Halle Volcanic Complex, Germany. *Journal of Petrology* **44**, 833–849.

Morgan, D. J. & Jerram, D. A. (2006). On estimating crystal shape for crystal size distribution analysis. *Journal of Volcanology and Geothermal Research* **154**, 1–7.

Morgan, S. (2018). Pascal's Principle, a Simple Model to Explain the Emplacement of Laccoliths and Some Mid-crustal Plutons. In: Burchardt, S. (ed.) *Volcanic and Igneous Plumbing Systems*. Amsterdam: Elsevier, 139–165.

Morgan, S., Stanik, A., Horsman, E., Tikoff, B., de Saint-Blanquat, M. & Habert, G. (2008). Emplacement of multiple magma sheets and wall rock deformation: Trachyte Mesa intrusion, Henry Mountains, Utah. *Journal of Structural Geology* **30**, 491–512.

Muir, D. D., Blundy, J. D. & Rust, A. C. (2012). Multiphase petrography of volcanic rocks using element maps: a method applied to Mount St. Helens, 1980–2005. *Bulletin of Volcanology* **74**, 1101–1120.

Mussett, A. E., Ross, J. G. & Gibson, I. L. (1980). $^{40}Ar/^{39}Ar$ dates of eastern Iceland lavas. *Geophysical Journal International* **60**, 37–52.

Palma, J. O., Burchardt, S., Galland, O., Schmiedel, T., Jerram, D. A., Mair, K. & Leanza, H. A. (submitted). *Structure and evolution of the shallow plumbing system of a back-arc volcano – The case of Chachahuén Volcano, Argentina*. .

Paquet, F., Dauteuil, O., Hallot, E. & Moreau, F. (2007). Tectonics and magma dynamics coupling in a dyke swarm of Iceland. *Journal of Structural Geology* **29**, 1477–1493.

Paterson, S. R. & Fowler, T. K. (1993). Re-examining pluton emplacement processes. *Journal of Structural Geology* **15**, 191–206.

Paterson, S. R., Fowler, T. K., Schmidt, K. L., Yoshinobu, A. S., Yuan, E. S. & Miller, R. B. (1998). Interpreting magmatic fabric patterns in plutons. *Lithos* **44**, 53–82.

Payacán, I., Gutiérrez, F., Gelman, S. E., Bachmann, O. & Parada, M. Á. (2014). Comparing magnetic and magmatic fabrics to constrain the magma flow record in La Gloria pluton, central Chile. *Journal of Structural Geology* **69**, 32–46.

Pérez, M. A. & Condat, P. (1996). *Geología de La Sierra de Chachahuén, Area CNQ-23*. Buenos Aires, Argentina.

Petford, N. (2009). Which effective viscosity? *Mineralogical Magazine* **73**, 167–191.

Pistone, M., Cordonnier, B., Ulmer, P. & Caricchi, L. (2016). Rheological flow laws for multiphase magmas: An empirical approach. *Journal of Volcanology and Geothermal Research* **321**, 158–170.

Pollard, D. D. & Johnson, A. M. (1973). Mechanics of growth of some laccolithic intrusions in the Henry mountains, Utah, II: Bending and failure of overburden layers and sill formation. *Tectonophysics*. Elsevier **18**, 311–354.

Preston, J. (2009). Tertiary igneous activity. In: Holland, C. H. & Saundes, I. S. (eds) *The Geology of Ireland*. Edinburgh: Dunedin Academic Press, 333–354.

Putirka, K. D. (2005). Igneous thermometers and barometers based on plagioclase + liquid equilibria: Tests of some existing models and new calibrations. *American Mineralogist* **90**, 336–346.

Putirka, K. D. (2008). Thermometers and Barometers for Volcanic Systems. *Reviews in Mineralogy and Geochemistry* **69**, 61–120.

Putirka, K. D. (2016). Amphibole thermometers and barometers for igneous systems and some implications for eruption mechanisms of felsic magmas at arc volcanoes. *American Mineralogist* **101**, 841–858.

Richards, J. P. (2003). Tectono-Magmatic Precursors for Porphyry Cu-(Mo-Au) Deposit Formation. *Economic Geology* **98**, 1515–1533.

Richey, J. E. (1928). The Structural Relations of the Mourne Granites, Northern Ireland. *Quarterly Journal of the Geological Society* **83**, 653–689.

Richey, J. E. (1961). *British regional geology: The Tertiary Volcanic Districts of Scotland*. Edinburgh: HMSO for the British Geological Survey.

Richey, J. E., Thomas, H. H., Radley, E. G., Dixon, B. E., Eyles, V. A., Lee, G. W., Radley, E. G. & Simpson, J. B. (1930). *The Geology of Ardnamurchan, North-West Mull and Coll (A Description of Sheet 51 and Part of Sheet 52 of the Geological Map)*. Edinburgh: HMSO for the British Geological Survey.

Ridolfi, F. & Renzulli, A. (2012). Calcic amphiboles in calc-alkaline and alkaline magmas: thermobarometric and chemometric empirical equations valid up to 1,130°C and 2.2 GPa. *Contributions to Mineralogy and Petrology* **163**, 877–895.

Ridolfi, F., Renzulli, A. & Puerini, M. (2010). Stability and chemical equilibrium of amphibole in calc-alkaline magmas: an overview, new thermobarometric formulations and application to subduction-related volcanoes. *Contributions to Mineralogy and Petrology* **160**, 45–66.

Riker, J. M., Cashman, K. V., Rust, A. C. & Blundy, J. D. (2015). Experimental Constraints on Plagioclase Crystallization during H_2O- and H_2O–CO_2-Saturated Magma Decompression. *Journal of Petrology* **56**, 1967–1998.

Rocchi, S., Westerman, D. S., Dini, A. & Farina, F. (2010). Intrusive sheets and sheeted intrusions at Elba Island, Italy. *Geosphere* **6**, 225–236.
Roni, E., Westerman, D. S., Dini, A., Stevenson, C. T. E. & Rocchi, S. (2014). Feeding and growth of a dyke–laccolith system (Elba Island, Italy) from AMS and mineral fabric data. *Journal of the Geological Society* **171**, 413–424.
Ruprecht, P. & Wörner, G. (2007). Variable regimes in magma systems documented in plagioclase zoning patterns: El Misti stratovolcano and Andahua monogenetic cones. *Journal of Volcanology and Geothermal Research* **165**, 142–162.
Saemundsson, K. (1979). Outline of the geology of Iceland. *Jökull* **29**, 7–28.
Sasvári, Á. & Baharev, A. (2014). SG2PS (structural geology to postscript converter) – A graphical solution for brittle structural data evaluation and paleostress calculation. *Computers & Geosciences* **66**, 81–93.
Schneider, C. A., Rasband, W. S. & Eliceiri, K. W. (2012). NIH Image to ImageJ: 25 years of image analysis. *Nature Methods* **9**, 671–675.
Scott, C. P., Allmendinger, R. W., González, G. & Loveless, J. P. (2016). Coseismic extension from surface cracks reopened by the 2014 Pisagua, northern Chile, earthquake sequence. *Geology* **44**, 387–390.
Senger, K., Buckley, S. J., Chevallier, L., Fagereng, Å., Galland, O., Kurz, T. H., Ogata, K., Planke, S. & Tveranger, J. (2015). Fracturing of doleritic intrusions and associated contact zones: Implications for fluid flow in volcanic basins. *Journal of African Earth Sciences* **102**, 70–85.
Sigmundsson, F. (2006). *Iceland Geodynamics, Crustal Deformation and Divergent Plate Tectonics*. Chichester: PraxisPublishing/Springer Berlin Heidelberg.
Sigmundsson, F. *et al.* (2015). Segmented lateral dyke growth in a rifting event at Bárðarbunga volcanic system, Iceland. *Nature* **517**, 191–5.
Smith, J. V. (2000). Textural evidence for dilatant (shear thickening) rheology of magma at high crystal concentrations. *Journal of Volcanology and Geothermal Research* **99**, 1–7.
Smith, J. V., Yamauchi, S. & Miyake, Y. (1993). Microshear zones in a Miocene submarine dacite dome of southwest Japan. *Bulletin of Volcanology* **55**, 438–442.
Snyder, G. L. & Fraser, G. D. (1963). Pillowed lavas, I. Intrusive layered lava pods and pillowed lavas, Unalaska Island, Alaska. *Geol. Surv. Prof. Paper 454-B*. Washington, D. C.: United States Government Printing Office, B1–B23.
Stevenson, C. T. E. & Bennett, N. (2011). The emplacement of the Palaeogene Mourne Granite Centres, Northern Ireland: new results from the Western Mourne Centre. *Journal of the Geological Society* **168**, 831–836.
Stevenson, C. T. E., Owens, W. H., Hutton, D. H. W., Hood, D. N. & Meighan, I. G. (2007). Laccolithic, as opposed to cauldron subsidence, emplacement of the Eastern Mourne pluton, N. Ireland: evidence from anisotropy of magnetic susceptibility. *Journal of the Geological Society* **164**, 99–110.
Stewart, A. L. & McPhie, J. (2003). Internal structure and emplacement of an Upper Pliocene dacite cryptodome, Milos Island, Greece. *Journal of Volcanology and Geothermal Research* **124**, 129–148.
Streck, M. J. (2008). Mineral Textures and Zoning as Evidence for Open System Processes. *Reviews in Mineralogy and Geochemistry* **69**, 595–622.
Terzaghi, R. D. (1965). Sources of Error in Joint Surveys. *Géotechnique* **15**, 287–304.
Thordarsson, T. & Höskuldsson, A. (2002). *Iceland: Classic Geology in Europe*. Terra, United Kingdom.
Torfason, H. (1979). Investigations into the structure of south-eastern Iceland. Doctoral dissertation, University of Liverpool, Liverpool.

Troll, V. R., Meade, F. C., Ganerød, M. & Chew, D. M. (2015). Short lived explosive volcanism in NE Ireland: rewriting the stratigraphy of the British and Irish Palaeogene Igneous Province. Irish Geological Research Meeting, Belfast, February 2015.

Tuffen, H., Dingwell, D. B. & Pinkerton, H. (2003). Repeated fracture and healing of silicic magma generate flow banding and earthquakes? *Geology* **31**, 1089.

Turner, S., George, R., Jerram, D. A., Carpenter, N. & Hawkesworth, C. (2003). Case studies of plagioclase growth and residence times in island arc lavas from Tonga and the Lesser Antilles, and a model to reconcile discordant age information. *Earth and Planetary Science Letters* **214**, 279–294.

van Wyk de Vries, B., Márquez, A., Herrera, R., Bruña, J. L. G., Llanes, P. & Delcamp, A. (2014). Craters of elevation revisited: forced-folds, bulging and uplift of volcanoes. *Bulletin of Volcanology* **76**, 875.

Walker, G. P. L. (1963). The Breiddalur central volcano, eastern Iceland. *Quarterly Journal of the Geological Society* **119**, 29–63.

Walker, G. P. L. (1966). Acid volcanic rocks in Iceland. *Bulletin Volcanologique* **29**, 375–402.

Walker, G. P. L. (1974). The structure of eastern Iceland. In: Kristiansson, L. (ed.) *Geodynamics of Iceland and the North Atlantic Area*. Dordrecht, Reidel, 177–188.

Walker, G. P. L. (1975). A new concept of the evolution of the British Tertiary intrusive centres. *Journal of the Geological Society* **131**, 121–141.

Waters, L. E. & Lange, R. A. (2015). An updated calibration of the plagioclase-liquid hygrometer-thermometer applicable to basalts through rhyolites. *American Mineralogist* **100**, 2172–2184.

Watkins, N. D. & Walker, G. P. L. (1977). Magnetostratigraphy of eastern Iceland. *American Journal of Science* **277**, 513–584.

Westerman, D. S., Rocchi, S., Breitkreuz, C., Stevenson, C. T. E. & Wilson, P. I. R. (2017). Structures Related to the Emplacement of Shallow-Level Intrusions. In: Breitkreuz, C. & Rocchi, S. (eds) *Physical Geology of Shallow Magmatic Systems. Advances in Volcanology (An Official Book Series of the International Association of Volcanology and Chemistry of the Earth's Interior)*. Springer, Cham, 83–118.

Wilson, P. I. R., McCaffrey, K. J. W., Wilson, R. W., Jarvis, I. & Holdsworth, R. E. (2016). Deformation structures associated with the Trachyte Mesa intrusion, Henry Mountains, Utah: Implications for sill and laccolith emplacement mechanisms. *Journal of Structural Geology* **87**, 30–46.

Wolfe, C. J., Th. Bjarnason, I., VanDecar, J. C. & Solomon, S. C. (1997). Seismic structure of the Iceland mantle plume. *Nature* **385**, 245.

Yang, H.-J., Kinzler, R. J. & Grove, T. L. (1996). Experiments and models of anhydrous, basaltic olivine-plagioclase-augite saturated melts from 0.001 to 10 kbar. *Contributions to Mineralogy and Petrology* **124**, 1–18.

Yoshinobu, A. S., Fowler, T. K., Paterson, S. R., Llambias, E., Tickyj, H. & Sato, A. M. (2003). A view from the roof: magmatic stoping in the shallow crust, Chita pluton, Argentina. *Journal of Structural Geology* **25**, 1037–1048.

Závada, P., Schulmann, K., Lexa, O., Hrouda, F., Haloda, J. & Týcová, P. (2009). The mechanism of flow and fabric development in mechanically anisotropic trachyte lava. *Journal of Structural Geology* **31**, 1295–1307.

Acta Universitatis Upsaliensis

Digital Comprehensive Summaries of Uppsala Dissertations from the Faculty of Science and Technology 1736

Editor: The Dean of the Faculty of Science and Technology

A doctoral dissertation from the Faculty of Science and Technology, Uppsala University, is usually a summary of a number of papers. A few copies of the complete dissertation are kept at major Swedish research libraries, while the summary alone is distributed internationally through the series Digital Comprehensive Summaries of Uppsala Dissertations from the Faculty of Science and Technology. (Prior to January, 2005, the series was published under the title "Comprehensive Summaries of Uppsala Dissertations from the Faculty of Science and Technology".)

Distribution: publications.uu.se
urn:nbn:se:uu:diva-363445

ACTA
UNIVERSITATIS
UPSALIENSIS
UPPSALA
2018